NTNU

Norwegian University of
Science and Technology

Unstable Gas Lift at the Heidrun Field

Sara Bjørkelund Haugen

Petroleum Geoscience and Engineering
Submission date: June 2017
Supervisor: Harald Arne Asheim, IGP

Norwegian University of Science and Technology
Department of Geoscience and Petroleum

Abstract

Gas lift is used in oil wells to maintain the production by injecting gas into the tubing. The dynamics of the system often causes pressure variations and a fluctuating flow rate.

Others have proposed design concepts for stable gas lift systems. However, measurements have been superficial and sparse and it has made it difficult to enable satisfactory verification of the concepts.

This thesis is based on flow rate, pressure and temperature data from a well at the Heidrun field in the Norwegian Sea. The measurements have been logged at a sufficient frequency to capture the most relevant dynamics. The well considered has periods where it produces evenly with a stochastic variation around $7\ \%$ and then it might suddenly change to oscillations with over $90\ \%$ deviation in the flow rate. The wavelength of the oscillations are $7 - 10\ \mathrm{min}$. Such shifts seams to occur without preceding disturbances, and it only affects the tubing pressure and flow rate, not the annular variables. This means, that casing heading is not the reason behind the oscillating behaviour.

A gas lift model has been implemented in Matlab to predict static changes in several variables, like phase fraction and pressure. Pressure predicted by this model compared to the measurement at Heidrun coincide with a maximum deviation of $2.3\ \%$.

A dynamical model based on an inflow correlation to simulate the well pressure was developed. The predictions was not consistent with the oscillations observed from the measurements, because the inflow correlation did not compare with the measured data.

The pressure response analysis did not show any sign of instabilities. However, an unstable well with oscillations was observed. The likely reason for the inconsistency is the casing heading assumption in the model. The large pressure drop across the downhole injection valve makes gas inflow insensitive to tubing variations, this decoupling prevents casing heading.

Sammendrag

Gassløft brukes i oljebrønner for å opprettholde produksjonen ved å injisere gass inn i røret. Dynamikken i systemet forårsaker ofte trykkvariasjoner og en oscillerende strømningshastighet.

Flere designkonsepter har blitt foreslått for stabile gassløftesystemer. Brønnmålinger har imidlertid vært overfladiske og sparsomme, og det har gjort det vanskelig å muliggjøre tilfredsstillende verifisering av konseptene.

Denne oppgaven er basert på strømningsrate-, trykk- og temperaturdata fra en brønn på Heidrunfeltet i Norskehavet. Målingene er logget med en tilstrekkelig frekvens for å fange den mest relevante dynamikken. Brønnen betraktet, har perioder der det produseres jevnt med en stokastisk variasjon rundt $7\ \%$, for så plutselig å endre til svingninger med over $90\ \%$ avvik i strømningshastigheten, med en oscillerende periode på $7 - 10\ \mathrm{min}$. Slike skift ser ut til å oppstå uten foregående forstyrrelser, og de påvirker bare brønntrykket og innstrømningsraten, ikke trykket eller gasstrømningsraten i ringrommet.

En gassløftmodell har blitt implementert i Matlab for å forutsi statiske endringer i flere variabler, som fasefraksjon og trykk. Sammenlignet med målingene i brønn A-23 ved Heidrun, sammenfaller trykket estimert av modellen med et maksimalt avvik på $2.3\ \%$.

En dynamisk modell basert på en innstrømningskorrelasjon for å simulere brønntrykket ble utviklet. Prediksjonen av denne modellen stemte ikke overens med svingningene observert, fordi innstrømningskorrelasjonen ikke stemte overens med målingene.

Trykkresponsanalysen viste ingen tegn på ustabilitet. Derimot, ble det observert en oscillerende ustabil brønn. Den sannsynlige årsaken til inkonsistensen er *casing heading* antagelsen i modellen. Det store trykkfallet over nedihullsinjeksjonsventilen gjør gassinnstrømning ufølsom til variasjoner i produksjonsrøret, dette forhindrer *casing heading* som ble antatt av modellen.

Acknowledgment

The master thesis presented is written during the spring 2017 as a part of the study program Petroleum Production at Norwegian University of Science and Technology (NTNU).

The Master Thesis is an extension of the project report "Gas Lift Instability - an Investigation at the Heidrun Field" written autumn 2016. The theory is based on the literature survey done in the project report. Flow rate, pressure and temperature data from well A-23 at Heidrun has been made available for examination in this thesis.

I would like to thank my supervisor Harald Arne Asheim for his great help during this year, it has been highly appreciated. I would also like to thank Statoil (operator of the Heidrun field) for providing well data and specifications. The view expressed in this paper is the views of me only and do not necessarily reflect Statoil's views.

Trondheim, June 11th 2017

Sara Bjørkelund Haugen

Contents

List of Figures

List of Tables

Chapter 1

Introduction

A gas lift installation is illustrated in Figure 1.1. Compressed gas is injected through the surface gas lift choke and into the annular space between the casing and tubing. The lift-gas flows down the annulus and enters the tubing through the downhole injection valve. The lift-gas mixes with the reservoir fluid, thereby reducing the density of the fluid mixture. Thereby decreasing the bottom-hole pressure and increasing the reservoir inflow.

Gas lift systems are usually designed assuring stable rates and pressures. However, field experience shows that instabilities and substantial variations sometimes occur. This may lead to several problems, such as mechanical issues in the production facilities, excessive use of lift-gas and a reduced production, which is obviously not beneficial.

Well A-23 at Heidrun experiences periodic variations in the pressures and flow rates. This leads to operational problems requiring the well to be shut-in occasionally. The purpose of the thesis was to analyze the pressure and flow rate variations. This was done by analyzing the frequency of the oscillations and by a stationary and dynamical model implemented in Matlab.

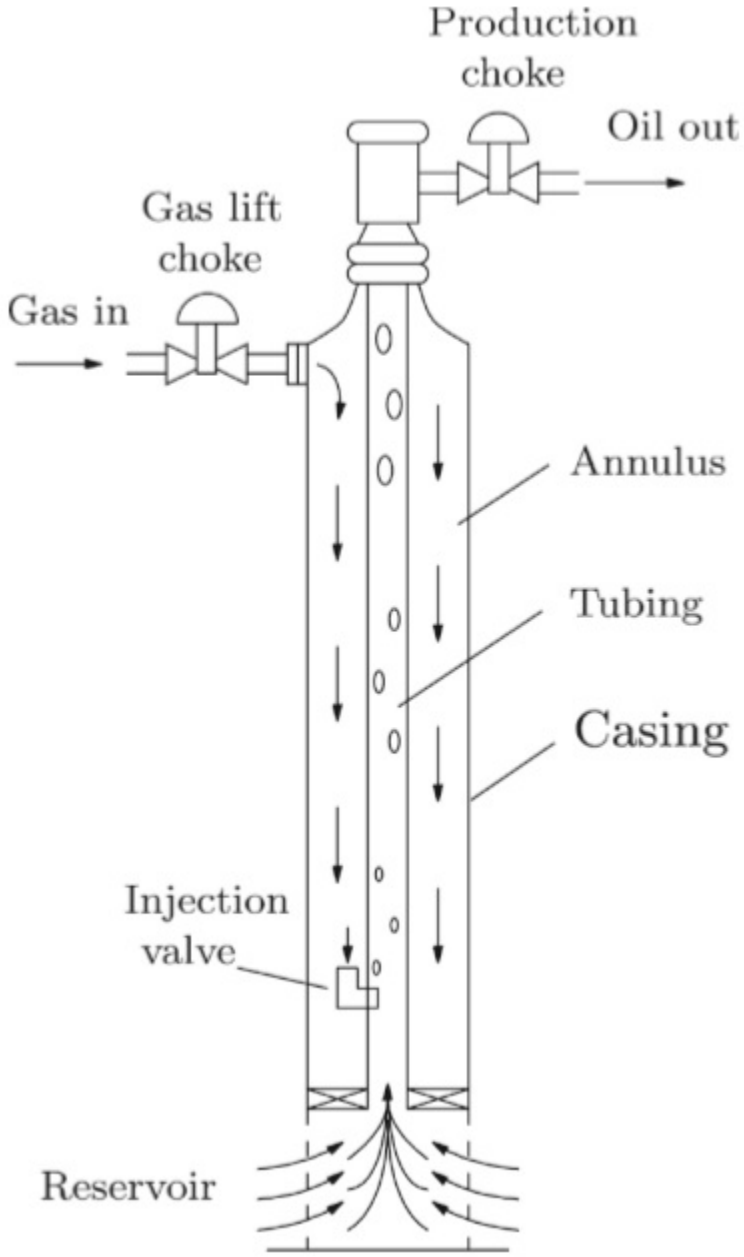

Figure 1.1: Sketch of a gas lift well (Eikrem et al., 2008)
Lift-gas is injected through the surface gas lift choke and into the annulus. Then the gas flows through the downhole injection valve and into the tubing where it mixes with the fluid in the tubing. This reduced fluid density decreases the tubing pressure and the reservoir inflow increases. The mixture fluid flows up the tubing and out through the production choke.

Chapter 2

Literature Survey

The literature survey presented in this chapter is an extension of the gas lift theory presented in the project report "Gas Lift Instability - an Investigation at the Heidrun Field."

2.1 The Concept of Gas Lift Instability

The unstable behaviour of a gas lifted well is often referred to as heading. The type of heading is determined based on where in the flow system the accumulation and discharge of free gas occurs, formation, casing and tubing heading are used in the literature (Xu and Golan, 1989).

In a gas lift system, as illustrated in Figure 1.1, changes in tubing pressure will change the pressure differential across the downhole injection valve, thus leading to a change in the gas inflow. Small changes can be caused by random disturbances from hydrodynamic slugs or by a temporal shutdown of the compressors (Larsen and Asheim, 2014; Fairuzov et al., 2004). Because the phase fraction in the fluid mixture reduces, the tubing pressure decreases and the gas inflow will continue to grow. As the gas inflow increases the gas supply cannot keep up and there is an imbalance between the gas flowing into the annulus and out through the downhole injection valve. This reduces the annular pressure and the pressure difference across the valve will be so low that there will be no flow of gas into the tubing. Because of the huge annular volume and the compressibility of gas, the annulus response is delayed and the well will experience a fluctuating behavior instead of a

stabilized flow (Hu and Golan, 2003). The concept described is referred as casing heading.

Kinematic waves, continuity waves and density waves are all names of the same reason of the occurrence of oscillating flow. This type of instability is different from heading, because the annular pressure and rate will behave constant, even though the flow rate and well pressure oscillates. The reason for the oscillations in the well parameters is that interface slippage causes liquid accumulation and a larger liquid holdup than liquid fraction. These holdup changes will propagate up the well as a density wave with a certain kinematic velocity (Hu and Golan, 2003; Asheim, 1999)

2.2 Stability criteria

Examining only inflow and outflow performance curves like Xu and Golan (1989) proposed is not sufficient for thoroughly examination of the stability of a gas lift well. Grupping et al. (1984a) and Grupping et al. (1984b) constructed a numerical model, however simple and reliable stability criteria are more applicable and easy to incorporate into the design phase. There have been proposed several stability criteria over the years, some of them are presented in the next subsections.

2.2.1 Blick et al. (1988)

Blick et al. (1988) created a model for unsteady flow in gas lift wells, that also can be modified for naturally flowing wells. The mathematical model considers well and reservoir variables that are affected by pressure fluctuations in the gas lift system. The basis is a series of differential equations expressing the pressure-dependent variables, which can be solved by Cramer's rule to obtain the

characteristic Equation's 2.1, 2.3, 2.4 with coefficients K_1, K_2 and K_3.

$$K_1 = (M_1 + M_2)\left(C_S - C_T + \frac{J}{ab}\right), \tag{2.1}$$

$$K_2 = \left[\left(\frac{\partial p_{th}}{\partial q}\right)_0 + \left(\frac{\partial \Delta p_1}{\partial q}\right)_0 + \left(\frac{\partial \Delta p_2}{\partial q}\right)_0\right]\left(\frac{J}{ab} + C_S\right) \tag{2.2}$$

$$+ J\,(M_1 + M_2) - C_T\left[\left(\frac{\partial \Delta p_1}{\partial q}\right)_0 + \left(\frac{\partial \Delta p_2}{\partial q}\right)_0\right], \tag{2.3}$$

$$K_3 = \left[\left(\frac{\partial p_{th}}{\partial q}\right)_0 + \left(\frac{\partial \Delta p_1}{\partial q}\right)_0 + \left(\frac{\partial \Delta p_2}{\partial q}\right)_0\right] J + 1, \tag{2.4}$$

where

$$M = \frac{\rho L}{A_t}, \qquad a = \frac{0.000264k}{\phi \mu c_f r_w^2}, \qquad b = \frac{0.892}{t_D^{0.792} r_{eD}^{0.217}}.$$

The subscript 1 represents the variables below the downhole injection valve, while subscript 2 considers variables above the downhole injection valve. The other symbols in these and the following equations are explained in the Nomenclature at page 68.

By using Routh's criteria (Smith and Corripio, 1997:chap 6-2.5) the model will predict stability for the well when the coefficients K_1, K_2 and K_3 of the characteristic equation in 2.1, 2.3 and 2.4 are of equal sign, thus, all positive or negative. However, if one or two of the coefficients have a different sign, the model will predict unstable well behaviour (Blick et al., 1988).

2.2.2 Asheim (1988)

Asheim (1988) developed two simple stability criteria, which provides a practical method for designing stable gas lift systems. The first criterion, seen in Equation 2.5 concerns the inflow response and the mixture-density-changes downhole where the gas is injected. According to this criterion the injection orifice must be small and the lift-gas flow rate and productivity index, J, must be high to have a stable gas lift system.

$$F_1 = \frac{\rho_g B_g Q_g^2}{Q_o} \frac{J}{(EA_i)^2} > 1. \tag{2.5}$$

The second criterion depends on pressure-depletion response. If the first criterion is not fulfilled, then a decrease in tubing pressure will cause increased inflow of lift gas and negative feedback will stabilize the flow. By this criterion in equation 2.6 the stability is promoted by a small annular volume, high injection gas flow rate and a high inflow-response ratio $\left(\frac{Q_o+Q_g}{Q_o}\right)$.

$$F_2 = \frac{V_t}{V_a}\frac{p_t}{\Delta\rho g L}\frac{(Q_o+Q_g)}{Q_o(1-F_1)} > 1. \tag{2.6}$$

The criteria only require information about variables used in the gas lift design, which is convenient because the optimum gas injection rate, tubing size and port size of the downhole valve can be decided. Alhanati et al. (1993) pointed out some limitations with Asheim's criteria in regards to the assumptions taken in the derivation of the two algebraic inequalities. Consequently, caution must be taken when using the criteria to determine stability.

2.2.3 Alhanati et al. (1993)

Alhanati et al. (1993) came up with another approach by deriving Asheim's criteria by the same mathematical techniques as Blick used. This illustrates that the differences between these criteria does not lie in the mathematical approach, but rather in the different models used to describe the behavior of the system components.

In a subcritical flow regime for both the downhole injection valve and the surface injection choke, which is the most common situation, Alhanati's criteria is

$$\left(F_1\frac{r_v}{\mu_v} - 1\right) + F_3\frac{2-r_v}{\mu_v}F_c > 0, \tag{2.7}$$

$$\left(F_1\frac{r_v}{\mu_v} - 1\right) + \frac{r_v}{F_c} > 0, \tag{2.8}$$

where F_1, F_3 and F_c is defined as

$$F_1 = \frac{\rho_g B_o Q_g^2}{Q_o}\frac{J}{(EA_i)^2}, \qquad F_3 = \frac{A_t p_t}{\Delta\rho g}\frac{(Q_o+Q_g)}{Q_o}, \qquad F_c = \frac{(EA_i)^2_{ch} + (EA_i)^2_v\left(\frac{r_{ch}(2-r_v)}{\mu_{ch}}\right)}{(EA_i)^2_v\left(\frac{r_{ch}(2-r_v)}{\mu_{ch}}\right)},$$

and

$$r_v = \frac{p_t}{p_{csg}}, \qquad \mu_v = \frac{(zT)_t}{(zT)_c},$$
$$r_{ch} = \frac{p_c sg}{p_m}, \qquad \mu_{ch} = \frac{(zT)_c}{(zT)_m}.$$

If the port size of the surface injection choke is small compared to the port size of the downhole valve, then $F_c \approx 1$ and Equation 2.7 and 2.8 would reduce to the equation for constant flow through the injection choke. This is a more general criteria than Asheim's, however it will reduce to Asheim's criteria under certain conditions.

Alhanati discovered that because of the simplifications taken when developing the criteria it could not predict all types of instabilities in gas lift wells. When the model was tested against field data, there were some instabilities in the well data that the model could not predict. These instabilities might have been caused by instabilities associated with vertical two-phase flow in pipes under certain conditions.

2.2.4 Aguilar et al. (2011)

Aguilar et al. (2011) investigated how water coning affects the stability in a gas lift well. Water coning is a rate-sensitive production problem which occurs near wellbore and reduces the oil production. Water from the reservoir infiltrates the perforations because the pressure forces dragging the water overcomes the buoyancy forces that segregates water from oil (Walsh, 2007:chap 9.11).

Based on Asheim's criterion in Equation 2.5, Aguilar extended the stability criterion to consider a different location for the perforations and the lift-gas injection point downhole. As a result, the criterion includes that the pressure at the injection point does not change immediately when the bottomhole pressure changes. Aguilar's criterion can then be written as

$$F_1 = \frac{\rho_g B_g Q_g^2}{Q_l} \frac{J}{(EA_i)^2} \frac{\partial p_w}{\partial p_i} > 1. \tag{2.9}$$

According to Aguilar, water coning may be a destabilizing factor in gas lift wells, because it can

lead to an increase in the liquid production which requires excessive gas injection to stabilize the well. In addition, unstable flow may accelerate water coning.

2.3 Well Design which Promotes Stability

According to the stability criteria it is possible to optimize the well design to promote stability. Some practical measures are choking the production by reducing the opening of the production choke or increasing the amount of injected gas by increasing the opening of the gas lift choke, but these are very inefficient operations. Re-completion and change of the tubing-size to decrease the tubing-casing annulus volume may also be considered, however, this is a very expensive alternative (Alhanati et al., 1993).

The downhole valve can be substituted with a valve with a smaller port size or with a venturi valve. The difference between an orifice valve and a venturi valve is that the square-edged orifice is replaced with a converging-diverging device seen in Figure 2.1. The converging-diverging nozzle reaches the critical flow condition at a lower downstream pressure than a normal square-edged nozzle, thus, prevents casing heading by keeping the gas injection rate constant (Tokar et al., 1996). However, it does not guarantee that the well will be stable and, moreover, the venturi valve hinders information from the tubing-annulus relation.

Even though the gas injection rate is kept constant, any phase fraction variation in the reservoir mixture flowing into the tubing will lead to a change in phase fraction in the two-phase mixture downhole. This phase fraction change may propagate upward the tubing as a kinematic wave and cause oscillating flow (Evers et al., 2009; Asheim, 1999).

The optimum method is to avoid gas lift instability as early as the design phase of the well. However, the anticipated well performance often deviates from the actual one. Thus, even a perfect design cannot guarantee a stable well, and other measures may be taken along the well life (Larsen and Asheim, 2014).

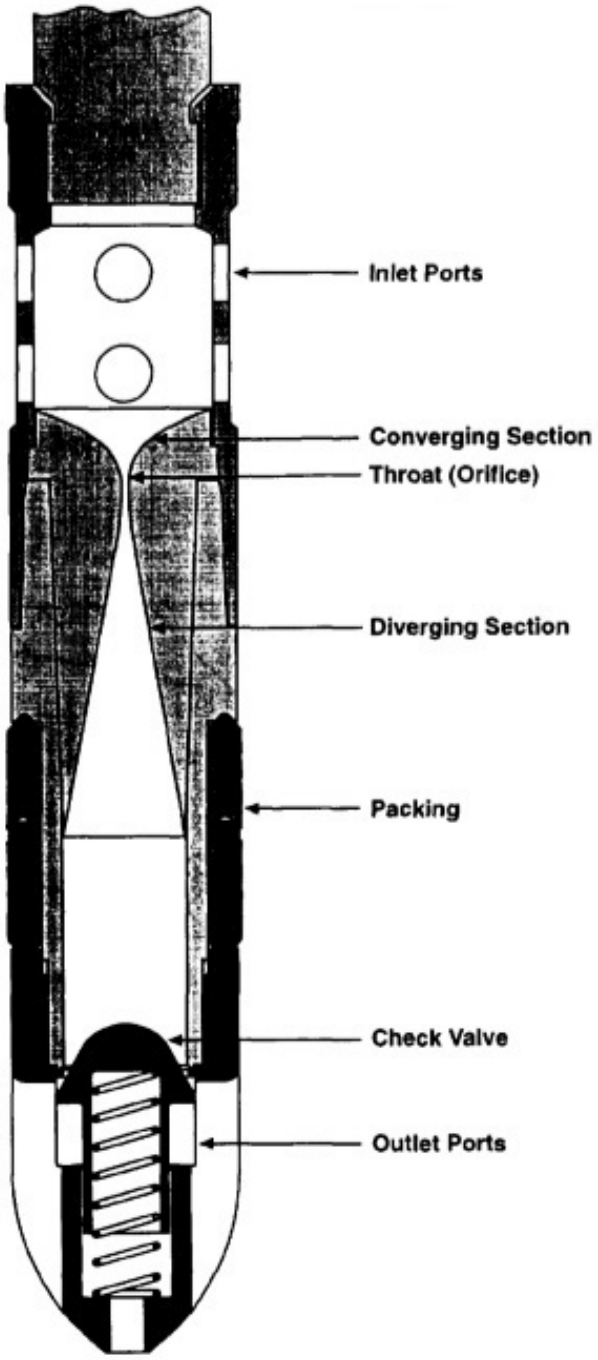

Figure 2.1: Cross-sectional sketch of a venturi valve (Tokar et al., 1996).
The lift-gas enters the valve through the inlet ports and passes through the converging section, the throat and the diverging section. Finally, the lift-gas exits through the outlet ports, and the check valve prevents reverse flow.

2.4 Stability Maps

Stability maps are 2D diagrams that shows the unstable and stable regions of the gas lift system, as well as the operational limits (Fairuzov et al., 2004). There are several parameters involved in the operating conditions in a gas lift well, however, usually there is only the size and depth of the gas lift orifice and gas injection rate that are unspecified. These three parameters span a 3D space, however, by fixating one of the parameters one obtain a 2D map instead.

2.4.1 Poblano et al. (2002)

Poblano et al. (2002) were the first ones to obtain stability maps for gas lift wells based on existing stability criteria. Asheim's and Alhanati's criteria were used, but others can be implemented.

Figure 2.2 illustrates a stability map based on Asheim's criteria. The dotted line illustrates the stability boundary, where the circles above represents the unstable conditions and the black triangles below are the stable conditions. The map shows that a low injection port size and a high gas injection rate is stabilizing. The map did not show any limitations for the lift-gas rate, which may be limited by the gas lift pressure or choking. The black filled circle represents the operating conditions of the unstable test well, the map confirms the unstable conditions.

Several advantages and applications for stability maps were proposed by Poblano:

- Compares different stability criteria.
- Can see the effects of tubing diameter, size and depth of the downhole gas injection valve and the gas injection rate.
- To find the well-stabilizing method that gives the minimum CAPEX (capital expense) and OPEX (operating expense).
- See where the unstable region is to design the system to operate far away from the stability boundary.

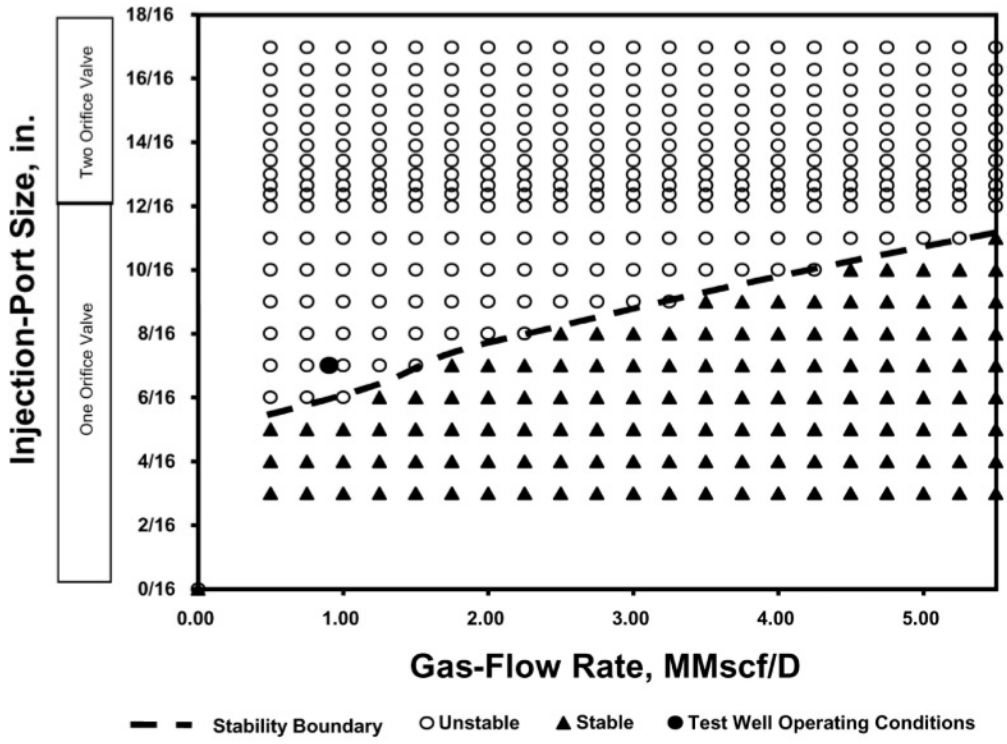

Figure 2.2: Gas lift stability map based on Asheim's criteria (Poblano et al., 2002).
The dotted line represents the stability boundary, where the circled points above shows instability and the triangles shows stable behaviour. The black filled circle is the operating conditions of the test well.

2.4.2 Fairuzov et al. (2004)

Fairuzov et al. (2004) investigated orifice size and depth, tubing inner diameter and inflow performance using stability maps based on Asheim's and Alhanati's criteria and Fairuzov's new criteria for saturated reservoirs. The new criteria predicts the stability boundary and regions more accurately.

The effects deducted from the stability maps showed that an increase in the productivity index was strongly stabilizing. Decreasing the annular volume is also stabilizing, however, this is usually accomplished by using a larger tubing inner diameter that will decrease the mixture velocity in the tubing, which can lead to a lower production rate or cause operational problems. An increase in gas injection valve depth will destabilize the system. The stability maps can be used to identify damaged wells and estimate the skin factor if the reservoir characteristics are known.

2.5 Feedback Control

By the definition of Dalsmo et al. (2002), feedback control means that the settings of one or more parameters in a system are based on readings of one or more measurements in the same system. This can be done both manually and automatically. In the case of gas lifted wells, measurements from tubing and annulus can be used and both the production choke and the gas injection choke can be automatically controlled. Feedback control can also be implemented in gas lift wells with dual completion (Eikrem et al., 2006).

2.5.1 Dalsmo et al. (2002)

Stabilization of a horizontal gas lift well at the Brage field was conducted by Dalsmo et al. (2002). Firstly, casing heading was eliminated by replacing the tubing with a smaller size and using a nozzle-venturi valve to obtain critical flow. However, the well still experienced erratic behaviour, maybe because of low rates which lead to separation of the fluid phases and, as a result, slugging. They used feedback control based on the production choke at the wellhead and a measurement of the downhole pressure as primary input to cope with the slugs. Active feedback control decreased the variations in the wellhead pressure by $75 - 100\ \%$ and there was not necessary to shut down the well to build up pressure.

2.5.2 Eikrem et al. (2006)

Some of the wells that use gas lift as an artificial method are producing with a dual completion tubing string. Often, the two tubing strings share a common gas lift supply, see Figure 2.3. Certain operating conditions, such as a sudden drop in tubing pressure, will cause difficulties with maintaining the injection of gas into both tubings. Instead, all of the lift gas will go through one tubing and this will most likely affect the oil production (Eikrem et al., 2006).

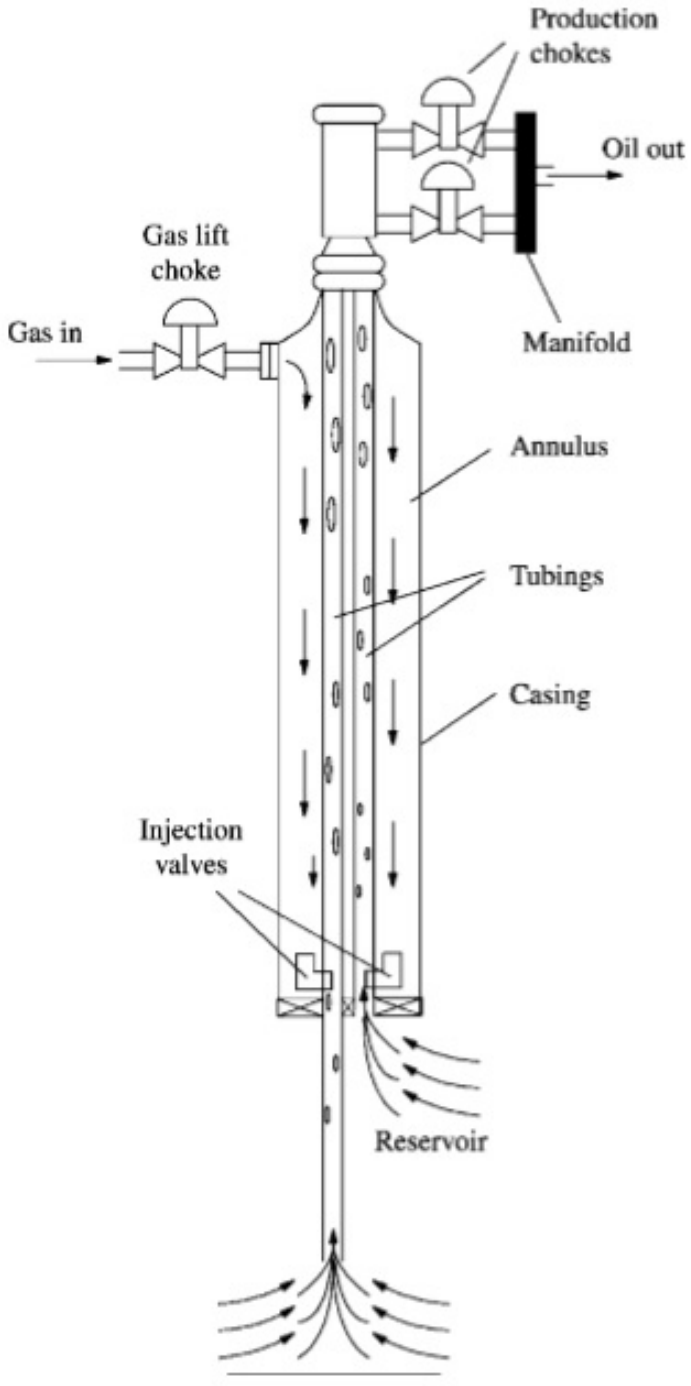

Figure 2.3: Sketch of a dual gas lift oil well (Eikrem et al., 2006).
The principle is the same as for a single gas lift oil well. However, since the two tubing strings share the same gas lift supply, problems with the lift-gas distribution can arise.

However, Eikrem presented a nonlinear dynamical model that captures the gas distribution instability. By using this model, stability maps can be created to show the desired setting ($\in [0, 1]$) for the production valve. The optimal production was shown to lie within the unstable region of the production valve settings. Which means that the gas distribution between the tubings cannot be obtained without automatic control. A simple control structure based on productivity index where suggested and it was able to stabilize the gas distribution instability both in simulators and laboratory experiments. In addition, the Nozzle-Venturi (NOVA) valve can be used to prevent robbing within the dual tubing (Tokar et al., 1996).

2.5.3 Eikrem et al. (2008)

Eikrem et al. (2008) investigated three different input parameters for the control structure, downhole pressure, casinghead pressure and differential pressure. Based on linear analysis, simulation by a simplified model and OLGA2000 and testing in an experimental laboratory setup, the investigation verified that all the control structures functioned. However, measurements based on the differential pressure experienced more noise in the experimental results than the other two measurements. Nevertheless, the results shows that several control structures can be applied and perform similarly for the same wells. This means that the control structure easily can be changed if a problem arises.

2.5.4 Larsen and Asheim (2014)

Gas lift stabilization by frequency control implies valve regulation to impose destructive interference. The concept is based on the fact that also stable wells are subjected to periodic variations. The natural frequencies in the stable periods can be determined by Fourier transformation, before they will develop into instabilities. Destructive interference may be imposed by periodic variation of the downhole injection valve or the tubing outlet choke. Larsen and Asheim (2014) investigated this concept experimentally in a scaled-down facility. Imposing oscillations reduced the pressure and flow variation up to 80-90$\%$ and increased the production rate up to 37$\%$. The scaled-down facility had the same static and dynamic behaviour as real wells, thus, the results may be reliable and a new control approach for gas lift instabilities may have been provided.

2.6 Comparing the Theories

All of the researchers presented in this thesis agrees that casing heading and instabilities caused by gas lift are more of a concern than a beneficial occurrence. There is also a consensus about the unpredictable behaviour and the requirement of constant evaluation of the producing wells. This is one of the reasons automatic control is being researched more.

The stability theories also agrees upon the actions that can be taken to stabilize the well. Such as decreasing the annulus volume, increasing the lift-gas flow rate, choking and substituting the downhole injection valve with a valve with smaller port size or with a converging-diverging nozzle. However, Dalsmo et al. (2002) and Hu and Golan (2003) have pointed out that choking and increasing the lift-gas injection are inefficient operations and implies expensive over-designs.

Several of the more recent criteria are based on Asheim (1988) criteria, which are easy to use and they only require well parameters from the gas lift design. However, the criteria are based on several assumptions, included neglecting friction and expansion. In addition, the criteria do only consider the inflow characteristics and how they respond to the downhole changes. Alhanati et al. (1993) criteria is based on many of the same assumptions as those Asheim used, including a gravity dominant tubing. Caution is necessary when using the criteria, however, they are still easy and useful, and they give a good estimate on the well behaviour.

Both Poblano et al. (2002) and Fairuzov et al. (2004) based their stability maps on Asheim's and Alhanati's criteria. According to Poblano, the criteria correlated with the observed conditions at their test well. On the contrary, Fairuzov believed that both the criteria underestimated the unstable region in the map. However, Asheim and Alhanati found their criteria to be conservative, which means that all the unstable conditions were found to be unstable within the tests, while the stable conditions were sometimes predicted as either stable or unstable by the criteria.A conservative approach can be used to assure operation under stable conditions, even though it might reject some operating conditions.

Chapter 3

Completion of Well A-23 at Heidrun

3.1 Development

The Heidrun oil and gas field is located in the Halten Terrace in the Norwegian Sea and is operated by Statoil Petroleum AS. The owners are Petoro AS (57.79 %), ConocoPhilips Skandinavia AS (23.99 %), Statoil Petroleum AS (13.04 %) and Eni Norge AS (5.18 %) (NorskPetroleum, 2017). Heidrun was discovered in 1985 by ConocoPhillips AS and has been producing since October 1995 (Statoil, 2015). The field has been developed with a floating concrete tension leg platform, which was installed above a subsea template with 56 well slots (NPD, 2016).

The reservoir consists of four different sandstone formations, where Garn and Ile have good reservoir quality and Tilje and Åre are somewhat more complex. The Garn and Ile formations are produced with both water and gas injection, unlike the more complex formations that mainly uses water injection for pressure support. However, well A-23 at Heidrun lies in the Åre formation and uses gas lift for recovery (NPD, 2016).

Statoil has signed an agreement with several other operators in the Norwegian sea to support their new discovers and the new developments. Heidrun will support the field Maria with water injection and support the gas field Dvalin with infrastructure and processing of the produced gas ("Norskehavskonferansen" 8.03.2017).

3.2 Completion

The completion of well A-23 at Heidrun is shown in Figure 3.1. The well is more or less vertical down to $1822\ \mathrm{m}$, where it starts deviating continuously with an angle of approximately $44°$. From here, all the lengths are given as measured depths. The gas lift valve is located at a measured depth of $1827\ \mathrm{m}$ while the gauge carrier, which does the bottomhole pressure measurement, is located at $2671\ \mathrm{m}$.

The casing reaches a measured length of $2913\ \mathrm{m}$, followed by sand screens and gravel pack down to $3023\ \mathrm{m}$. The well penetrates the pay zone with an average angle of $33°$. The reservoir section has a height of $147\ \mathrm{m}$, where the top of the reservoir starts at $2905\ \mathrm{m}$ and the bottom is at $3052\ \mathrm{m}$.

The produced fluid flows up the tubing, through the wellhead and out through the production choke. The multiphase measurements are located around the outlet. The lift-gas pressure and rate are regulated at the gas lift choke at the lift-gas inlet. The lift-gas flows down the annulus and through the downhole gas lift valve into the tubing. It is important to account for the fact that the lift-gas mixes with the producing fluid around $1000\ \mathrm{m}$ above the reservoir.

3.3 Well Specifications

The well specifications from Statoil's completion scheme and the PVT-data are given in Table 3.1. The oil density, oil viscosity and oil formation factor are in reservoir conditions. The reservoir pressure is also stated in the table, even though it is estimated from a buildup test in Chapter 7.2.

The well produces an average of $277\ \mathrm{Sm^3/day}$ oil and $643\ \mathrm{Sm^3/day}$ water. Since gas is injected into the well the average gas produced is $157,190\ \mathrm{Sm^3/day}$, where $71,734\ \mathrm{Sm^3/day}$ comes from the reservoir and the remaining amount of $85,457\ \mathrm{Sm^3/day}$ is the lift-gas. This gives a water-oil-rate, WOR, of $2.32\ \mathrm{Sm^3/Sm^3}$ and the total gas-oil-ratio, GOR, is $567\ \mathrm{Sm^3/Sm^3}$ while the reservoir GOR is $259\ \mathrm{Sm^3/Sm^3}$.

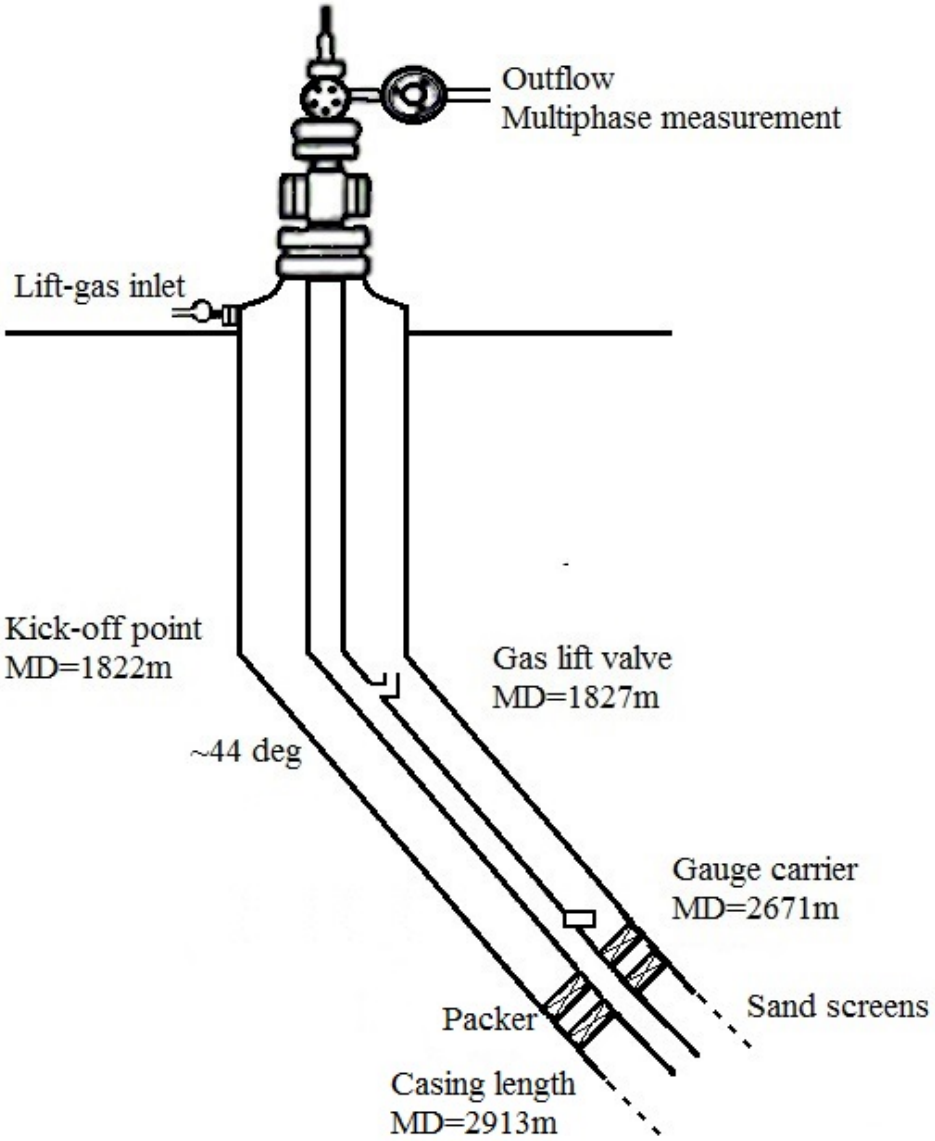

Figure 3.1: Sketch of the completion at well A-23 at Heidrun.

Table 3.1: Well Specification Parameters

Description	Parameter	Value
Gravity	g	$9.81\ \mathrm{m/s^2}$
Reservoir temperature	T	$85\ ^\circ\mathrm{C}$
Injection depth	L_i	$1828\ \mathrm{m}$
Measurement depth	L_{mfm}	$2671\ \mathrm{m}$
Casing depth	L_r	$2913\ \mathrm{m}$
Tubing inner diameter	ID_t	$0.1214\ \mathrm{m}$
Tubing outer diameter	OD_t	$51/2$ "
Casing inner diameter	ID_{csg}	8.54 "
Orifice opening	ID_{valve}	$23/64$ "
Reservoir pressure	p_r	$171 \times 10^5\ \mathrm{Pa}$
Gas gravity	γ_g	0.606
Oil density	ρ_o	$834.9\ \mathrm{kg/m^3}$
Oil viscosity	μ_o	$0.2868\ \mathrm{Pa \cdot s}$
Oil formation factor	B_o	$1.143\ \mathrm{m^3/Sm^3}$

Chapter 4

Stationary Gas Lift Model

A stationary system is often used to quantify if a gas lift design is stable. Any flow is subjected to external disturbances or noise, and such variations may be amplified under certain conditions.

Before creating a model where the oscillations and the time delay between the bottomhole and the wellhead is considered, a stationary model that operates by averaging the rates and pressure over a certain time period is developed.

4.1 Annulus

The general pressure balance is $dp + \rho g dh + dF = 0$, where dF is the friction loss. By integrating this expression along the pipe and setting $dF \approx 0$ and $\rho = \frac{pM}{zRT}$, the pressure in a static gas column becomes

$$p_a = p_g e^{\frac{MgL}{zRT}}. \tag{4.1}$$

By using Taylor series to develop a linear approximation of the exponential, Equation 4.1 can be re-written as

$$\frac{p_a}{p_g} = 1 - \left(\frac{MgL}{zRT}\right) + \frac{1}{2}\left(\frac{MgL}{zRT}\right)^2 - \frac{1}{2 \times 3}\left(\frac{MgL}{zRT}\right)^3 + \cdots. \tag{4.2}$$

When the expression in the parenthesis is much smaller than 0, approximately 10^{-6} in this case, Equation 4.2 can be simplified to

$$p_g = p_a \left(1 - \frac{MgL}{zRT}\right) \tag{4.3}$$

$$\rightarrow p_a = p_g + \rho_g g L \tag{4.4}$$

since $\frac{M}{zRT} = \rho_g / p_a$.

For well A-23 at Heidrun it is assumed that the annular space is gas filled from the wellhead and down to the injection point and water filled beneath. This is reasonable because there is a much higher risk for the tubing to burst or the casing to collapse if the annulus is filled completely with gas.

Equation 4.4 is only valid for a column of gas, thus, it does not apply for the column below the injection point. The pressure for the bottom of the annulus can be expressed by integrating the pressure gradient equation, but without the friction term since there is no production in the annulus. The pressure in the bottom of the annulus is expressed as

$$p_a = p_{ai} + \rho_w g L. \tag{4.5}$$

4.2 Tubing

The gas lift system involves both flow through the annulus and the tubing. For the current analysis, valves, reservoir and other interacting parts are assumed to react immediately to the imposed disturbances, thereby behave as constant parameters.

Starting with the tubing response and the pressure gradient at steady flow in Equation 4.6, where the friction term is valid for an incompressible fluid:

$$\frac{dp_t}{dx} + \rho_{tp} g + \frac{1}{2} f \frac{\rho_{tp} v_m^2}{d} = 0. \tag{4.6}$$

Integrating the pressure drop along the tubing, the bottomhole pressure can be expressed as

$$p_{wf} = p_{wh} + \overline{\rho}_{tp} g + \frac{1}{2} f_{tp} \frac{\overline{\rho}_{tp} \overline{v}_m^2}{d} L. \tag{4.7}$$

Assuming that the produced fluids flows into a pressure controlled separator, a constant wellhead pressure, p_{wh} can be considered.

The impact from friction and slippage, in addition to gas expansion and the location of the gas lift valve causes a pressure dependence through the whole tubing. This is why the pressure drop has to be integrated stepwise from wellhead to bottomhole, where all the varying variables (density, velocity and friction factor) can be accounted for.

4.3 Gas Expansion

Gas is compressible and will expand as the pressure decreases upwards the tubing. Oil is slightly compressible and as the oil moves upwards the tubing, soluble gas will come out of the solution.

The oil, gas and water formation volume factors, $B_o,\ B_g,\ B_w$, converts the oil, gas and water from surface conditions to bottomhole conditions (Whitson and Brulé, 2000). B_w will be neglected since it is always close to 1 (Schlumberger, 2016). To estimate B_o and B_g, Standing (1947) correlation must be used to estimate the soluble gas at downhole conditions seen in Equation 4.8:

$$R_s = 0.00590 \gamma_g \times 10^{\frac{2.14}{\gamma_o} - 0.000198T} (0.797 p_t + 1.4)^{1.205}. \tag{4.8}$$

The oil formation factor can be calculated from Standing (1947) Equation 4.9, and the gas formation volume factor can be calculated from volume changes in the general gas equation $pV = znRT$ seen in Equation 4.10 (Whitson and Brulé, 2000:pp. 25-35).

$$B_o = 0.9759 + 0.952 \times 10^{-3\left(\left(\frac{\gamma_g}{\gamma_o}\right)^{0.5} R_s + 0.401T - 103\right)^{1.2}} \tag{4.9}$$

$$B_g = \left(\frac{p_{sc}}{T_{sc}}\right) \frac{zT}{p_t}. \tag{4.10}$$

p_{sc} and T_{sc} are estimated by Sutton (1985) correlations and Yarborough and Hall (1974) equation of state is used to find the z-factor. Both Sutton (1985) correlation and Yarborough and Hall (1974) equation of state requires the reservoir pressure, which can be estimated by a buildup test, which will be executed in Chapter 7.2.

4.4 Flow Friction

The Darcy-Weisbach friction factor is a dimensionless quantity that describes friction losses in pipe flow. The two-phased friction factor is estimated by a correlation of Blasius (1913):

$$f = A \times Re^{-B}, \tag{4.11}$$

where A and B are the friction factor correlation parameter and exponent, respectively, and Re, Reynolds number, is defined as

$$Re = \frac{\rho_{tp} v_m d}{\mu_{tp}}.$$

Al-Shemmeri (2012) equation of temperature dependent water viscosity, in Equation 4.12, is used to estimate how the water viscosity changes along the tubing in the fluid mixture. The accuracy of the water viscosity prediction lies within $2.5\ \%$ (Al-Shemmeri, 2012:p. 17)

$$\mu_w = 2.414 \times 10^{-5} \times 10^{\frac{247.8}{T-140}}. \tag{4.12}$$

The change in oil viscosity through the tubing was estimated by given PVT-properties from Statoil. A constant composition expansion laboratory test was performed as a part of the PVT-analysis, where the oil viscosity was measured at various pressures, illustrated in Figure 4.1. The equation for the polynomial trendline, which is created to fit the points in Figure 4.1, is given in Equation 4.13. This equation represents a relationship between the oil viscosity and the pressure in well A-23 at Heidrun.

$$\mu_o = 6 \times 10^{-5} p_t^2 - 0.0301 p_t + 6.3348, \quad \text{where} \quad R^2 = 0.9425. \tag{4.13}$$

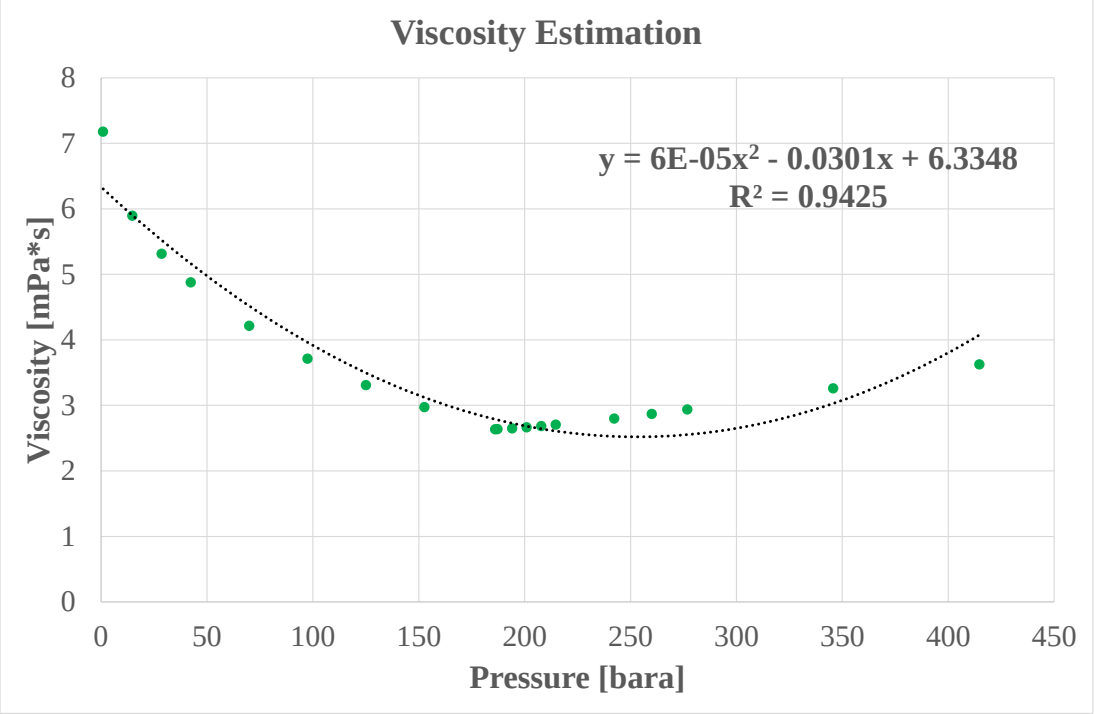

Figure 4.1: Oil viscosity estimation from Statoil data.
Oil viscosity and pressure data from Statoil were used to estimate a pressure dependent equation for the oil viscosity.

The R-squared value, $R^2 = 0.9425$, is quite near 1, resulting in a good correlation between the trendline and the datapoints.

4.5 Slippage

Slippage is a term governing the friction between gas and liquid. Since gas has a smaller density and viscosity than the liquid, it will usually flow faster. Drift flux models provide relationships between superficial velocities and liquid fraction. There exist several hold up relations, such as the original drift flux model by Zuber and Finlay (1965), relating the gas velocity with total superficial velocity:

$$v_g = C_o v_m + v_d, \quad \text{where} \quad v_m = v_{sl} + v_{sg}.$$

where v_d is either the rise velocity of bubbles or sink velocity of droplets. Since the expression for gas velocity is $v_g = \frac{Q_g}{A_g} = \frac{v_{sg}}{y_g}$ and the relationship between gas and liquid fraction is $y_l = 1 - y_g$, an expression of the liquid fraction related to the superficial velocities can be obtained:

$$y_l = 1 - \frac{v_{sg}}{C_o(v_{sg} + v_{sl}) + v_d}.$$

This hold up model is widely used, however, it can be misleading. Asheim (1986) model relates gas velocity directly to the liquid velocity, instead of the total superficial velocity. Since Asheim (1986) hold up expression given in Equation 4.14 is more applicable, it will be used in this thesis.

$$y_l = \frac{1}{2}\sqrt{\left(\frac{v_{sg}}{v_0} + C_0\frac{v_{sl}}{v_0} - 1\right)^2 + 4C_0\frac{v_{sl}}{v_0}} - \frac{1}{2}\left(\frac{v_{sg}}{v_0} + C_0\frac{v_{sl}}{v_0} - 1\right), \tag{4.14}$$

where C_o is the gas distribution factor and v_o is the drift velocity. The superficial velocities can be expressed by the specific fluid flow over the cross-sectional tubing area, for instance $v_{sl} = Q_l/A_t$. If both fluids flows upwards the tubing, Equation 4.14 will have one solution between 0 and 1.

Neglecting slippage implies that Equation 4.14 reduces to

$$y_l = v_{sl}/v_m. \tag{4.15}$$

However, neglecting slippage will probably result in an underestimation of the liquid fraction.

4.6 Inflow from Reservoir

The injected gas flow rate is given by the lift-gas rate measurement. Many wells with gas lift installed operates with a fixed gas injection rate. The average value of the lift-gas flow rate from well A-23 will be used.

Since the water-oil-ratio, WOR, is very high, both water and oil needs to be considered, thus $Q_l = Q_o + Q_w$ is used. The productivity index is given by the liquid inflow performance (Walsh, 2007:p.

700):

$$J = \frac{Q_l}{p_r - p_{wf}}. \tag{4.16}$$

The liquid mixture density is given by $\rho_l = \rho_o \frac{Q_o}{Q_l} + \rho_w \left(1 - \frac{Q_o}{Ql}\right)$. The two-phased density used in Equation 4.7 considers the gas and liquid fraction, which can be found in Equation 4.14. The two-phased density can be written as

$$\rho_{tp} = y_l \rho_l + (1 - y_l)\rho_g. \tag{4.17}$$

4.7 Comparison with the Well Measurements at Heidrun

The model is tested against the data from Heidrun to confirm the models credibility. In January 2017, seen in Figure 7.2 in Chapter 7.1.1, the well seems to have a stable production with some noise in the measurements of pressure and rates, a shut-in period and periods with highly oscillating production. The shut-in period can be used to estimate the reservoir pressure. Data from the stable and unstable period will be used to verify the stationary model. In addition, stable and highly oscillating periods in November and December in Figure 7.1 and several other periods from the data set, seen in Appendix A, will be used to optimize the model.

Pressure and rates for a stationary case are estimated by averaging the pressure and rate data. For the period from January 1st to 18th the averaged variables are seen in Table 4.1. When adjusting the model to apply for the situation at Heidrun the gas distribution factor, C_o were set to be equal to 1.296 and the drift velocity equal to $0.2\ \mathrm{m/s}$.

Table 4.1: Well Parameter Measurements January 2017

Description	Parameter	01.01-18.01.2017
Tubing head pressure	p_{th}	22.3 bar
Tubing pressure	p_t	122.5 bar
Gas injection pressure	p_g	118.9 bar
Liquid rate	Q_l	$819.7\ \mathrm{Sm^3/day}$
Total gas rate	Q_g	$138,470\ \mathrm{Sm^3/day}$
Lift-gas rate	Q_{gi}	$88,506\ \mathrm{Sm^3/day}$

A pressure and velocity profile are created for the averaged parameters of the first 18 days in

January 2017. The averaged parameters are stated in Table 4.1. The profiles can be seen in Figure 4.2 and 4.4. In addition, the gas-liquid fraction propagation is plotted in Figure 4.3.

In Figure 4.2 the wellbore pressure in blue and the annulus pressure in red are plotted against the tubing length. The wellbore pressure is estimated by using the pressure gradient in Equation 4.7. The estimated tubing pressure is $122.7\ \mathrm{bar}$ and the measured one is $122.5\ \mathrm{bar}$. The annulus is assumed to be gas-filled from the top down to the injection valve and liquid-filled below. The three dotted lines represents the depth of the gas injection valve in red, the gaige carrier in green and the reservoir in magenta. The pressure in the bottom of the well (top of reservoir) is approximately $140\ \mathrm{bar}$ while the pressure in the reservoir is $171\ \mathrm{bar}$.

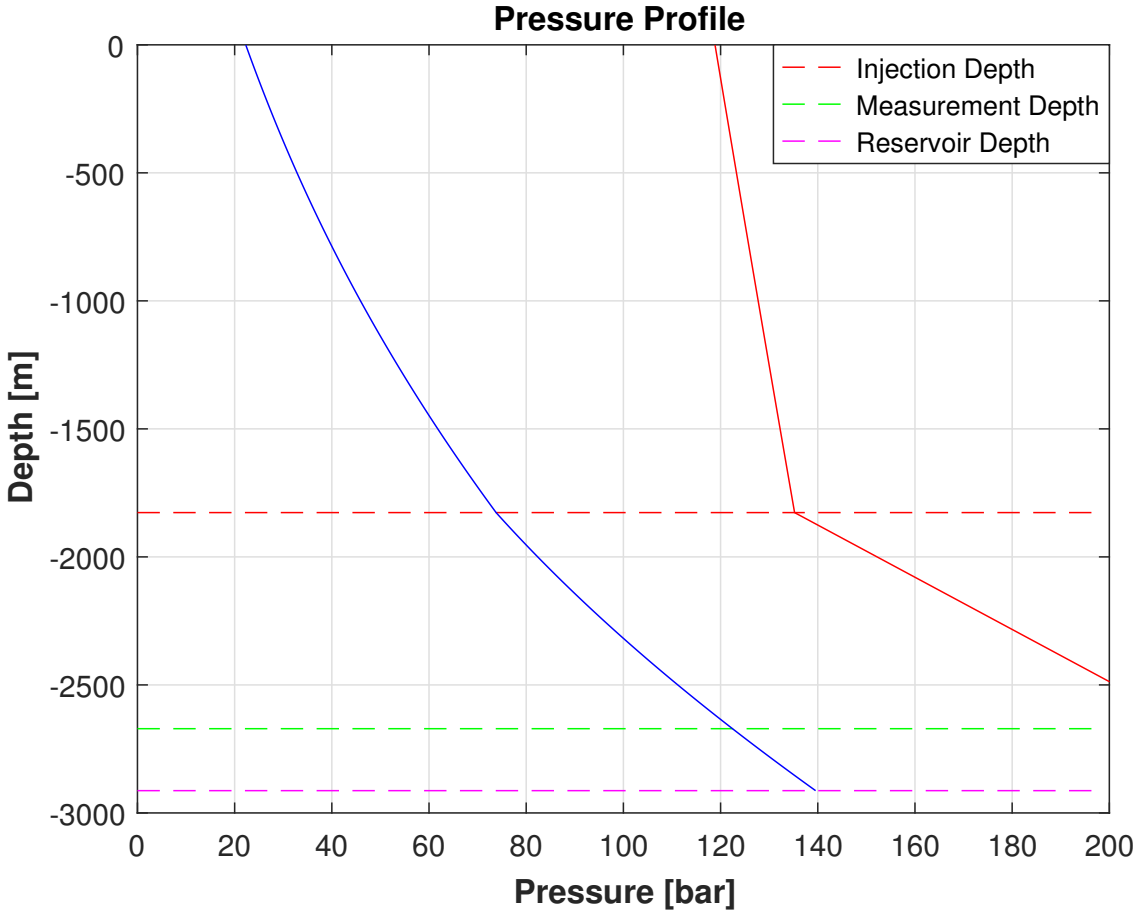

Figure 4.2: Pressure profile.
Wellbore pressure in blue and annulus pressure in red. The annulus is gas-filled from the injection point and up to the wellhead and liquid-filled down to the reservoir. The difference between the wellbore pressure and the annular pressure at the injection depth is not consistent with the choke flow equation 4.18.

The pressure differential between the annulus and the tubing should satisfy the choke flow relationship:

$$p_a - p_t = \frac{1}{2}\rho_g \frac{Q_g^2}{A_i^2}, \tag{4.18}$$

the derivation of this equation is given in Appendix B.

At the point of gas injection, that is the dotted red line in Figure 4.2, the tubing pressure is $p_t = 73.8\ \mathrm{bar}$ and the annular pressure is $p_a = 135.2\ \mathrm{bar}$. This equals a difference of $61.4\ \mathrm{bar}$. On the other hand, the estimated parameters at the gas injection valve are $\rho_g = 93.2\ \mathrm{kg/m^3}$, $Q_g = 0.0082\ \mathrm{m^3/s}$ and $A_i = 6.54 \times 10^{-5}\ \mathrm{m}$, which equals a pressure differential of $7.3\ \mathrm{bar}$ according to Equation 4.18. The estimated pressure drop from Figure 4.2 and the calculated from Equation 4.18 is not consistent.

The liquid fraction propagation is seen in Figure 4.3. The plot has the same layout as Figure 4.2. The blue line is the liquid fraction, which decreases with tubing depth. Since $y_g = 1 - y_l$, the gas fraction is approximately 0.86 at the tubing head and 0.25 at the reservoir depth. Gas comes out of the liquid solution and an additional amount is injected at the injection depth, this is why the liquid fraction increases and the gas fraction decreases with depth.

In Figure 4.4 the superficial velocity of liquid and gas are plotted against the tubing length. The dotted lines represents the reservoir, the gauge carrier and the gas injection valve depth. The liquid superficial velocity in orange does not change significantly through the tubing. In contrast, the gas superficial velocity in blue has a constant slope from the inlet until the gas injection valve where the velocity increases exponentially to the tubing head. The gas superficial velocity depends on the gas rate, which increases as the gas expands upwards the tubing.

Too small velocity can cause liquid accumulation in the bottom of the well, this can also happen to the produced sand. On the other hand, a too large velocity can damage equipment by accelerating corrosion or, if the velocity is extremely high, it can also cause erosion.

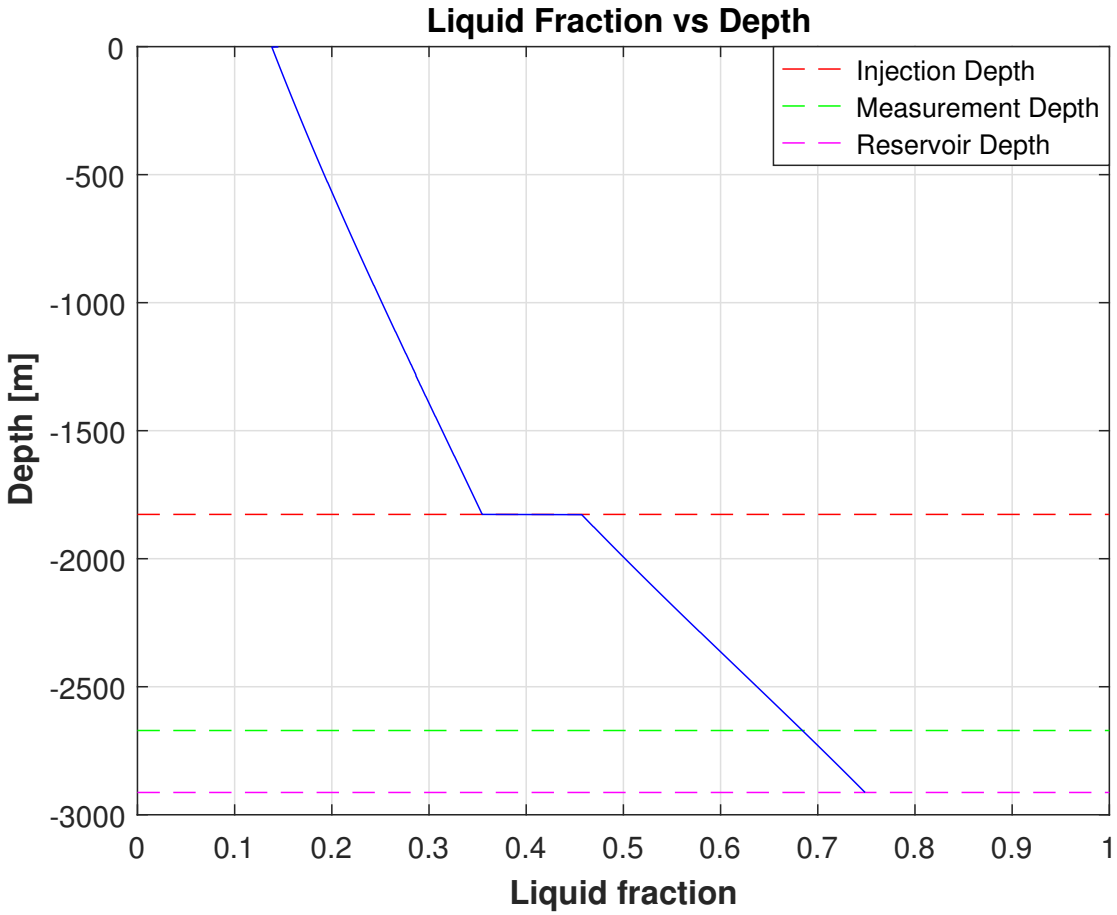

Figure 4.3: Liquid fraction.
The liquid fraction increases with depth, while the gas fraction decreases with depth. This is due to gas expansion and gas injection.

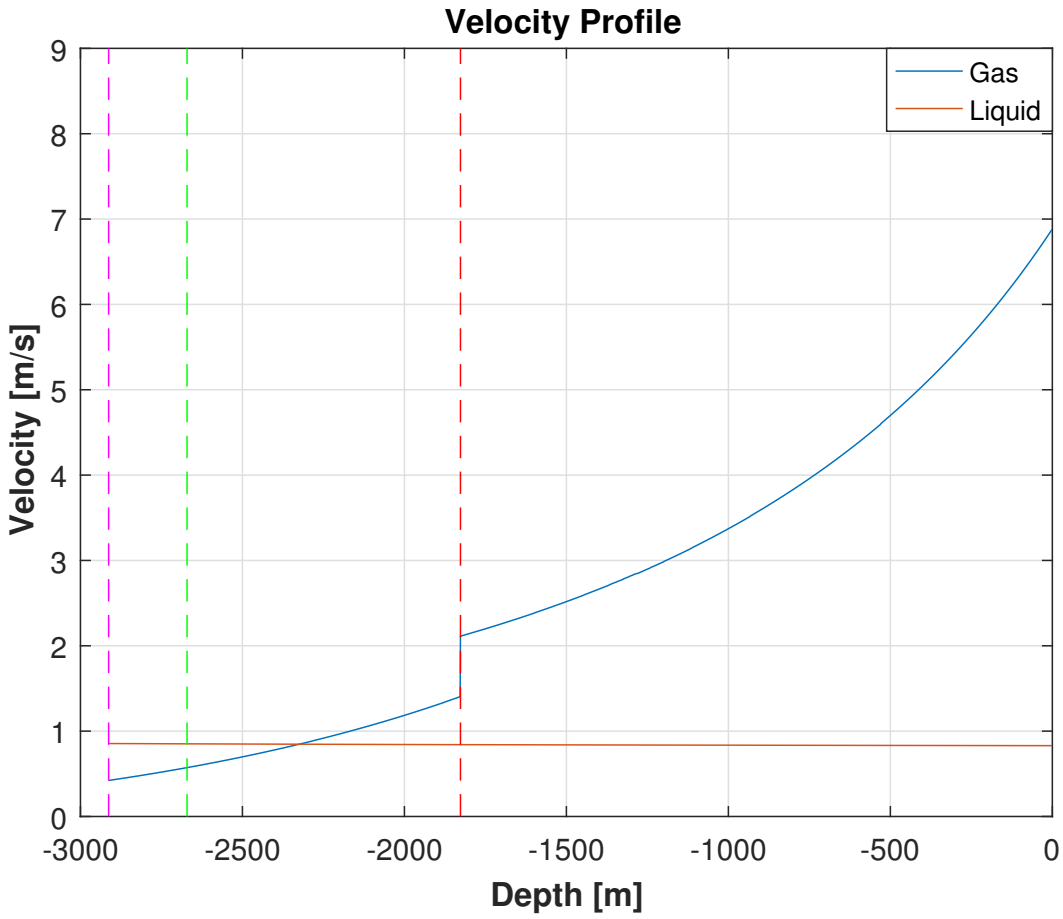

Figure 4.4: Velocity profile.
The dotted lines represents the reservoir, measurement and injection depth. The liquid superficial velocity is more or less constant, while the gas superficial velocity increases constantly until the gas injection point, where it starts increasing exponentially.

Chapter 5

Dynamical Gas Lift Model

The dynamical gas lift model uses a modified version of the stationary model in Chapter 4 to simulate how the pressure and rate develops over time. The given values from the well specification will be used, in addition, the wellhead temperature will be prefixed at $55\ ^{\circ}C$. The bottomhole pressure and wellhead pressure will be simulated.

Since the variables is not averaged over an entire period as in the stationary period, the model can be used over time to illustrate the well behaviour.

5.1 Annulus

The gas injection rate is often dependent on the well pressure. However, for well A-23 at Heidrun, the gas injection pressure and rate are controlled on the surface in the gas lift choke, and the well data will be used for these variables in the model.

5.2 Flow Across the Injection Valve

The pressure in the annulus is estimated in the same way as was done in Chapter 4.1. The pressure differential between the annulus and the tubing across the downhole injection valve is used to find

the tubing pressure at the injection valve, seen in Equation 5.1.

$$p_{ti} = p_{ai} - \frac{1}{2}\rho_{ga}\frac{Q_{ga}^2}{A_i^2}. \tag{5.1}$$

The estimated pressure drop did not correspond with the calculated one in Chapter 4.7. Thus, for the dynamical model, the size of the orifice port will be adjusted. Equation 5.1 can be written as

$$A_i = \sqrt{\frac{1}{2}\frac{\rho_{ga}Q_{ga}^2}{p_{ai} - p_{ti}}} = \frac{\pi}{4}ID_{valve}^2. \tag{5.2}$$

To calculate the port size that is consistent with the simulation, parameters at the gas injection depth from Chapter 4 is used, the density of gas, gas injection rate, annular and well pressure. The orifice port size corresponding with the choke flow equation and the simulated case is $0.0053\ \mathrm{m}$, which is within the range of a typical orifice port size, and is then reasonable to use in the dynamical model. Then it will be possible to estimate the well pressure at the gas injection depth by using the choke flow relationship in Equation 5.1.

5.3 Tubing

The pressure above and below the injection point can be estimated from the well pressure given by 'Equation 5.1 at the injection point in the tubing. Equation 4.7 from Chapter 4.2 will be used to estimate the well pressure from the injection point and down to the reservoir. From the injection point and up to the wellhead, equation 5.3 will be used.

$$p_t = p_{ti} - \overline{\rho}_{tp}g - \frac{1}{2}f_{tp}L\frac{\overline{\rho}_{tp}\overline{v}_m^2}{d}L. \tag{5.3}$$

The principle of gas expansion, flow friction, slippage and propagation is the same for the stationary case in Chapter 4 and the dynamical case.

5.4 Inflow From Reservoir

The inflow from the reservoir can be estimated in several different ways. Firstly, the given flow rate data of the outflow can be used when accounting for the phase delay. Secondly, an inflow performance correlation can be obtained regarding the inflow and the altering bottomhole pressure.

5.4.1 Flow Rate Data with Time Delay

The parameters will propagate up the tubing with a kinematic velocity. The time delay between fluid fraction being generated at the well bottom and appearing at the tubing head can be estimated by

$$\Delta t = \frac{L}{v_c}, \quad \text{where} \quad v_c = C_o v_m. \tag{5.4}$$

The kinematic velocity can be estimated from the stationary model.

In addition, to account for possible uncertainties in the multiphase measurements, an exponential moving mean of the flow rate measurements will be used.

5.4.2 Inflow Performance Relationship

A simple inflow performance relationship (IPR) based solely on the estimated productivity index, the previous calculated bottomhole pressure and the reservoir pressure can estimate the flow rates:

$$Q_o = J_o \left(p_r - p_{wf}^{old}\right) \tag{5.5}$$

$$Q_w = J_w \left(p_r - p_{wf}^{old}\right) \tag{5.6}$$

$$Q_g = r * Q_o, \tag{5.7}$$

where J_o and J_w are the productivity index for oil and water, and r is the gas-oil-ratio of the inflow from the reservoir.

The productivity indexes are based on data from one measurement at the wellhead and one measurement for the tubing pressure at Δt before the surface measurements. The measurements at the

wellhead are used to simulate the propagation of the variables in the tubing. The estimated pressure at the gauge carrier depth can then be compared to the measured pressure at $-\Delta t$. When these two matches, the estimated pressure can be extrapolated downhole and the bottomhole pressure can be used to estimate the productivity index J_o and J_w.

Chapter 6

Dynamical Response

One can use the criteria presented in Chapter 2.2 to determine whether the flow will be unstable or not based on the parameters from the stationary or dynamical model. However, the criteria have their limitations. The criteria consider inflow response and dynamic response for annulus and tubing, but the criteria does not consider the outflow characteristics. One of the most general models covering both inflow and outflow response is the differential equation, seen in Equation 6.1, developed by Asheim (2016).

$$\frac{\partial}{\partial t}\begin{bmatrix}\delta p_{wf}\\ \delta p_g\end{bmatrix} = \begin{bmatrix}a_w & -a_g\\ c & -c\end{bmatrix}\begin{bmatrix}\delta p_{wf}\\ \delta p_g\end{bmatrix}_t + \begin{bmatrix}d_w & -d_g\\ 0 & 0\end{bmatrix}\begin{bmatrix}\delta p_{wf}\\ \delta p_g\end{bmatrix}_{t+\Delta t} \tag{6.1}$$

neglecting the delayed outflow response $t + \Delta t$, the matrix simplifies to

$$\frac{\partial}{\partial t}\begin{bmatrix}\delta p_{wf}\\ \delta p_g\end{bmatrix} = \begin{bmatrix}a_w & -a_g\\ c & -c\end{bmatrix}\begin{bmatrix}\delta p_{wf}\\ \delta p_g\end{bmatrix}_t \tag{6.2}$$

The differential Equation 6.1 can be used to simulate how the pressure will respond to a disturbance, δ, considering both inflow and outflow response. The equation is solved by the ode45 solver in Matlab. If an initial disturbance of $\delta p_{wf} = 1$ Pa and $\delta p_g = -1$ Pa are applied on the pressure response, the flow rate will also vary, since it is pressure dependent. If the oscillations imposed by the disturbance increases with time, the system is dynamical unstable.

The coefficients $a_w,\ a_g,\ c,\ d_w,\ d_g$ of matrix 6.1 can be determined by the well parameters and the derivations are given in Appendix B. The coefficients are dependent of several types of responses:

$$
\begin{aligned}
a_w &= \alpha \left(J_g K_g - J K_l + F_g J_g^2 K_a \right) \\
a_g &= \alpha \left(J_g K_g + F_g J_g^2 K_a \right) \\
c &= J_g K_a \\
d_w &= \alpha \left(J_g K_g - J K_l \right) \\
d_g &= \alpha J_g K_g \\
\alpha &= \left(1 + F_g J_g + F_l J \right)^{-1},
\end{aligned}
$$

where K_g and K_l means density response to gas and liquid flow, F_g and F_l means friction response along tubing to gas and liquid flow and the K_a is an annular pressure response relation. J is the usual productivity index and J_g is the gas injection index.

Chapter 7

Dynamical Behaviour at Well A-23

7.1 Well Behaviour

7.1.1 Overview of the Production

The data provided by Statoil from well A-23 at Heidrun are obtained every minute from January 1st 2016 00:00:00 to February 22nd 2017 00:00:00. The data used are tubing, wellhead and gas lift pressure, bottomhole and wellhead temperature, gas lift rate and the multiphase flow rate measurements of oil, water and total gas.

The oscillating behaviour at Heidrun is seen in Figure 7.1 for November and December 2016 and in Figure 7.2 for January 2017 to February 22nd 2017. The black curves are the liquid rate measured every minute. The red curves are the exponential moving average. In the parts where the flow rate oscillates with a high amplitude, the exponential moving mean also have a high amplitude compared to the more evenly producing periods.

There are a great difference between the amplitude of the oscillations in these four months. November has very large oscillations with a maximum of $4794\ \mathrm{Sm}^3/\mathrm{day}$, while almost all of January, 19 of 31 days, have a low amplitude. The maximum rate in January is $2781\ \mathrm{Sm}^3/\mathrm{day}$.

Well A-23 experiences oscillating flow and slugs. Comparing the size of the oscillations in Novem-

ber in Figure 7.1 and in January in Figure 7.2, one clearly see a difference from the highly oscillating periods and the ones characterized by a more stable production. The problematic behaviour has led to shut-in periods. Statoil have tried to adjust the lift-gas rate and the production choke opening, however, they have not seen a clear effect on the oscillations and they still struggle with the behaviour.

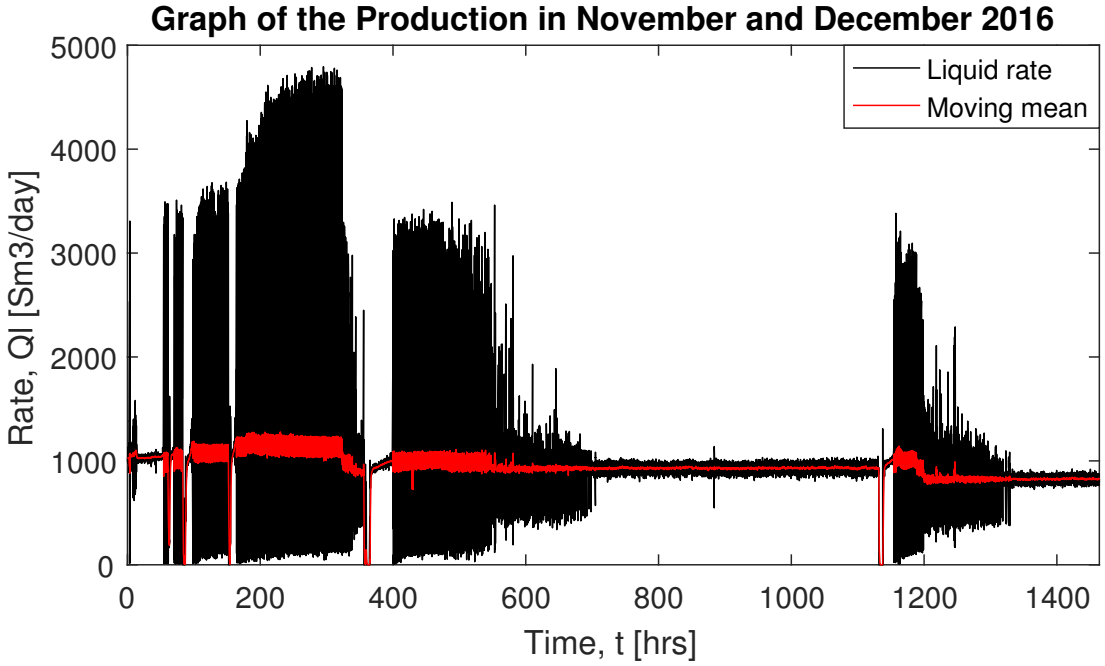

Figure 7.1: Liquid production in November and December.

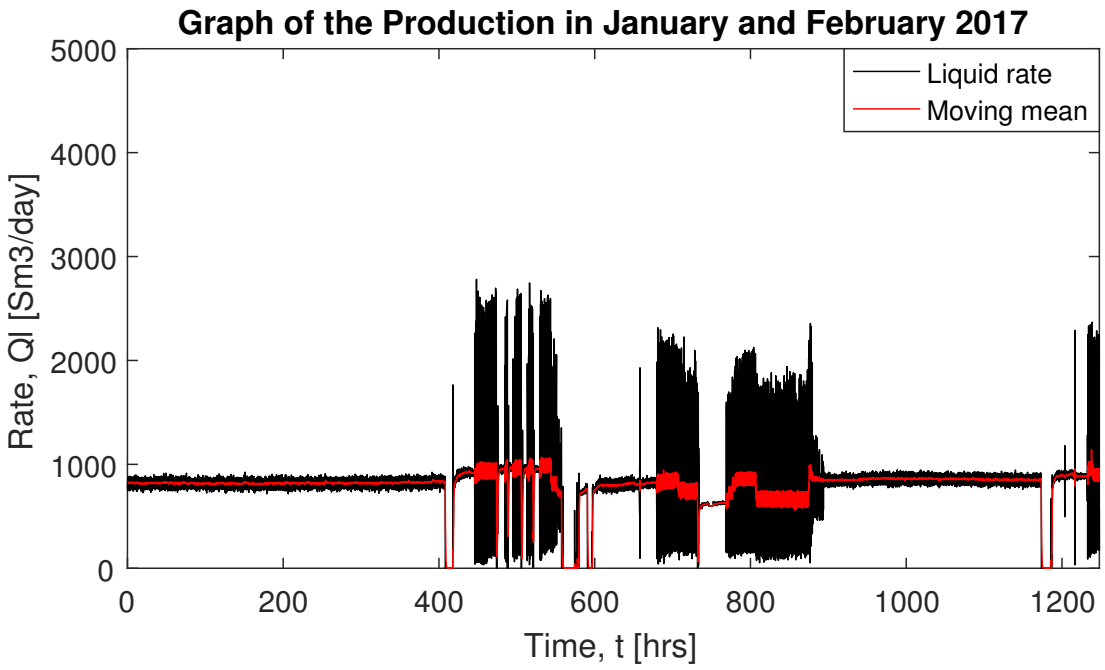

Figure 7.2: Liquid production in January until February 22nd 2017.

7.1.2 Periods Characterized by Noise and Oscillations

Figure 7.3 and 7.4 are plots of the liquid rate over 5 hours in one low and one highly oscillating period. The mean value is plotted in blue, the exponential moving mean in magenta and the standard deviation in red.

Figure 7.3 is divided into two plots, which illustrates 6 hrs of the production on January 1st 2017. The top plot has the same scale as the plot in Figure 7.4, this shows the amplitude difference in the oscillations in the stable and unstable periods. The data used in the top and bottom plot are the same in Figure 7.3, however, the bottom plots y-axis is reduced from $Q_l \in (0, 3000)$ $\mathrm{Sm}^3/\mathrm{day}$ to $Q_l \in (750, 900)$ $\mathrm{Sm}^3/\mathrm{day}$. This makes it possible to see how the rate develops and how small the deviation from the mean is. The liquid rate does not fluctuate with a constant frequency or period, the fluctuations are quite irregular.

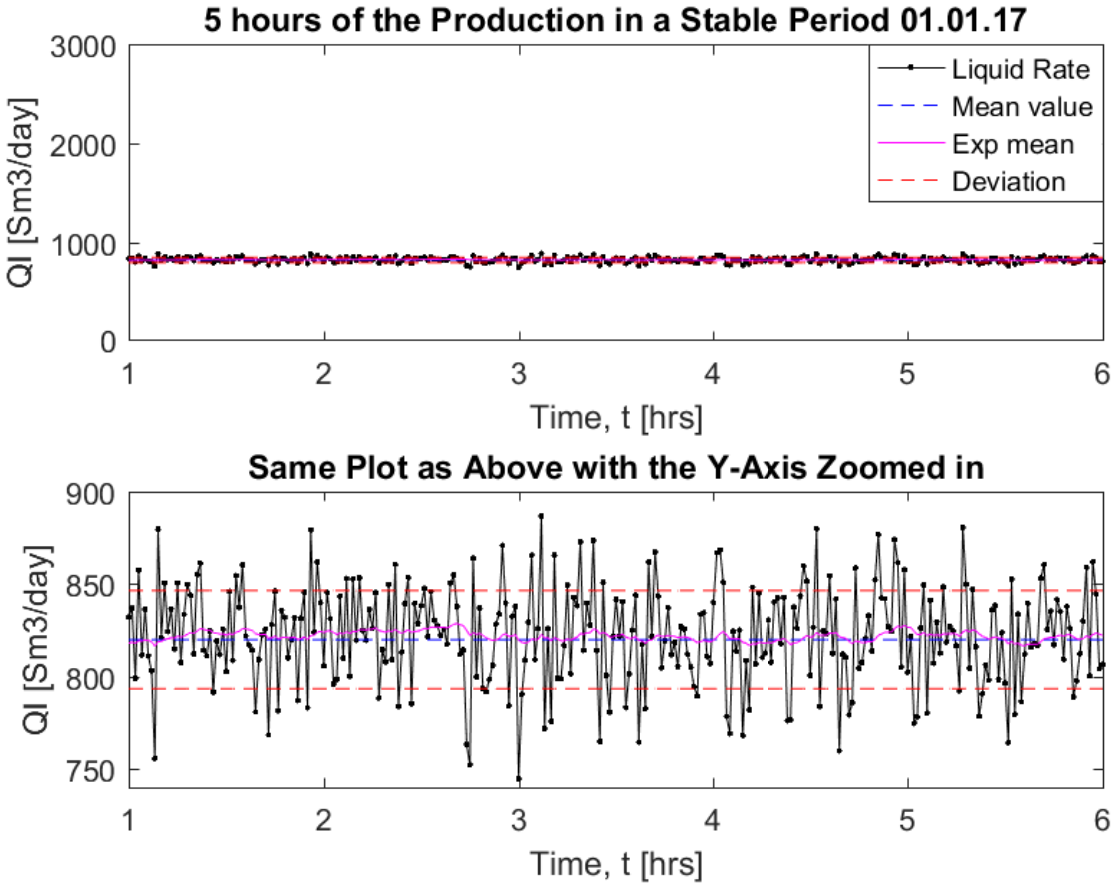

Figure 7.3: Liquid production during a 5 hours period on January 1st.
The top plot is an overview of the production, it shows that the fluctuations are very small compared to the highly oscillating periods. The bottom plot zooms in on the y-axis and displays the behaviour of the flow rate, which is irregular.

The fluctuations in Figure 7.4 oscillates with what seems to be a constant frequency and period, but with some difference in the amplitude of each oscillation. In contrast to Figure 7.3 the deviation from the mean is extremely high, 790 compared to $26\ \mathrm{Sm}^3/\mathrm{day}$.

Figure 7.5 illustrates the cumulative distribution around the mean value of the liquid rate of the first $400\ \mathrm{hrs}$ in January 2017 in the top plot. The mean rate is $819\ \mathrm{Sm}^3/\mathrm{day}$ and the standard deviation is $26.5\ \mathrm{Sm}^3/\mathrm{day}$. The blue lines are one standard deviation, σ, the dashed lines are 2σ, the dotted lines are 3σ and so on. Despite the erratic behaviour seen in Figure 7.3, the rate is evenly distributed around the mean value. The probability of the rate being very small or very high is low.

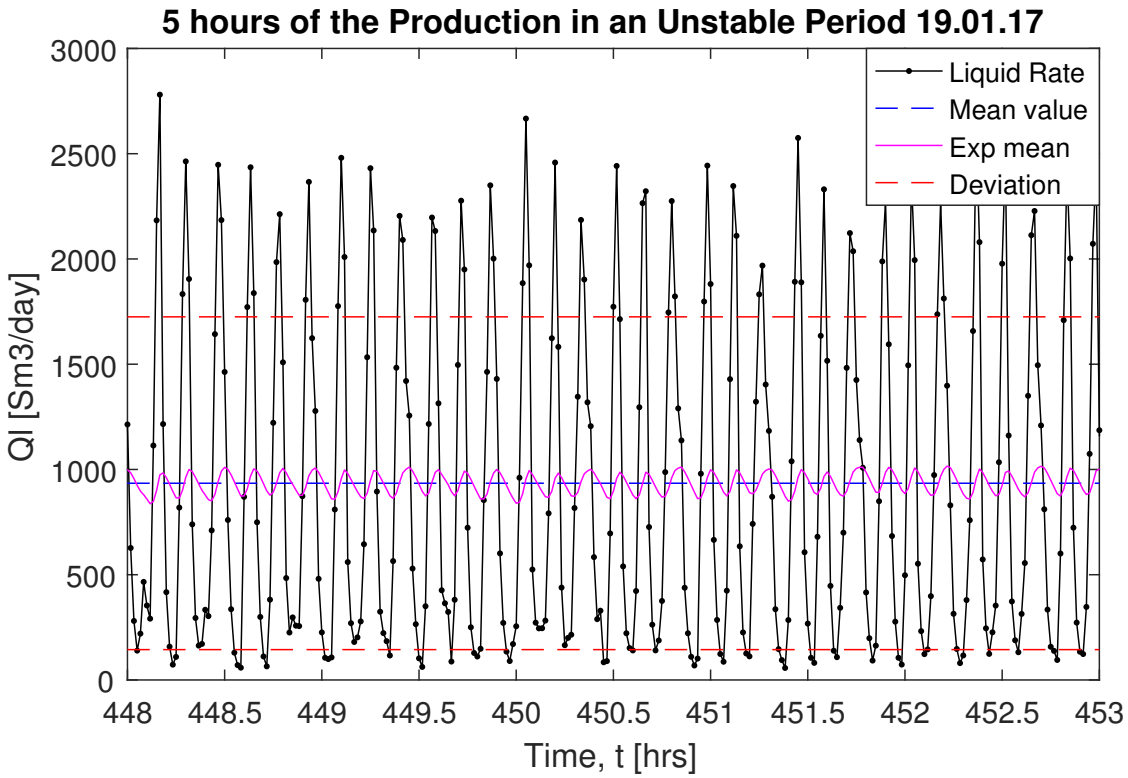

Figure 7.4: Liquid production during a 5 hours period January 19th.
The rate is highly oscillating with a standard deviation of 790 $\mathrm{Sm}^3/\mathrm{day}$.

The bottom plot in Figure 7.5 covers a highly oscillating period over 26 hours on January 19th to 20th. Unlike the curve in the top plot, the curve for the highly oscillating period is not normally distributed. The probability of the rate being small and close to the standard deviation is high. The high rates, on the other hand, can be both close to the standard deviation or far of.

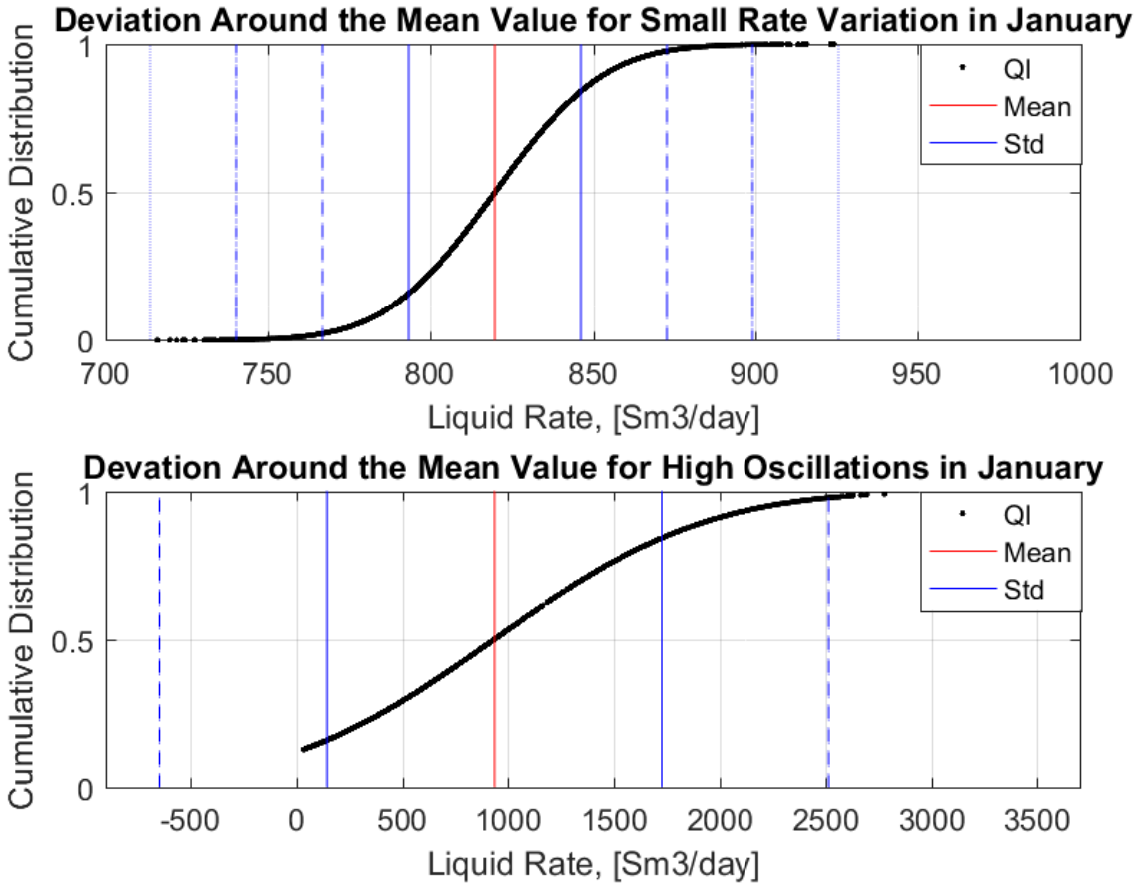

Figure 7.5: Cumulative distribution of periods with both small and high oscillations. The top plot illustrates that the liquid rate is distributed normally around the mean value.

7.1.3 Transition between the Production Profiles

The sudden change between a steadily producing period with irregular, normally distributed variations in well pressure and flow rate to a highly oscillating production profile is illustrated in Figure 7.6 over the time interval $t \in (444, 452)$ hrs. The top plot represents the wellhead pressure in green, the pressure at the gauge carrier in red and the gas lift pressure in magenta. The bottom plot shows the liquid flow rate in black, the total gas rate in yellow and the lift-gas rate in magenta. The gas flow rates have been divided by 200 and 100, respectively, to display the interaction between the flow rates in a clearer manner.

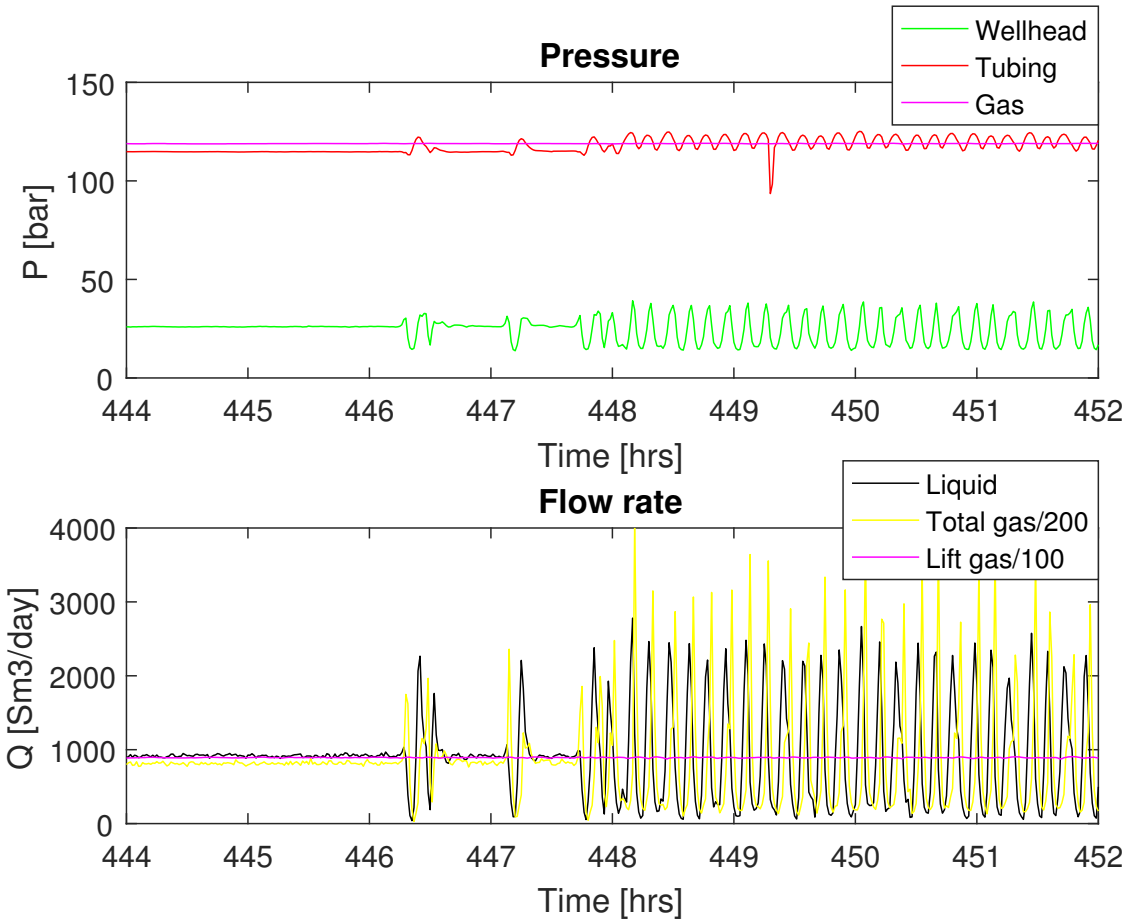

Figure 7.6: Transition between the steadily producing and highly oscillating period.

Both the gas lift pressure and the lift-gas rate are more or less constant in the whole time interval, while the other variables starts oscillating vigorously right before $t = 448$ hrs. It seems like the oscillating period is about to start right after $t = 446$ hrs and $t = 447$ hrs, but the variables returns to the initial state after two and one wavelengths in these situations. There is no clear difference in the parameters in the beginning of these two short oscillating periods and the long oscillating period from right before $t = 448$ hrs. There is also no visible reason for why the two first oscillating periods returns to the initial state immediately unlike the long oscillating period. In addition, the opening of the production choke and the gas lift choke were kept constant during this time.

7.2 Buildup Test

In January 2017, that is the first half of Figure 7.2, ($t \in (0, 744)$ hrs), there are what seems to be both stable and unstable production in addition to a couple of shut-in periods. The reservoir pressure can be estimated from the shut-in period, this is also called a buildup test. Since the bottomhole pressure is measured approximately 242 m above the reservoir, the pressure gradient for this length needs to be manually added to the measurement.

In Figure 7.7, a buildup test is plotted. The test works by closing the well, so there will be no flow and the well pressure will gradually build up to the average reservoir pressure (Fekete-Associates-Inc., 2012).

Figure 7.7 illustrates the liquid rate, the measured well pressure and the estimated reservoir pressure. The black curve, the liquid flow rate, is zero in the shut-in period, thus the well is not producing. The red curve is the measured bottomhole pressure at the point of the gauge carrier at 242 m above the reservoir. The blue line represents the measured well pressure plus the pressure between the measuring point and the reservoir. The pressure differential between the measuring point and the reservoir is calculated by the liquid pressure equation, $p = \rho g L$, where the density in the reservoir is used. After the well has been shut-in for 10 hrs, the pressure reading show a reservoir pressure of approximately 171 bar.

The pressures in Figure 7.7 experiences an initial transient, seen in the peek at $t = 408 - 410$ hrs. This transient consist of the first reaction the pressure has after the well stops producing, which is an increase, before it decreases. At $t = 410$ hrs the well pressure gradually increases and reaches the buildup pressure at steady-state. An initial transient often occurs as a start-up period before the steady-state is achieved.

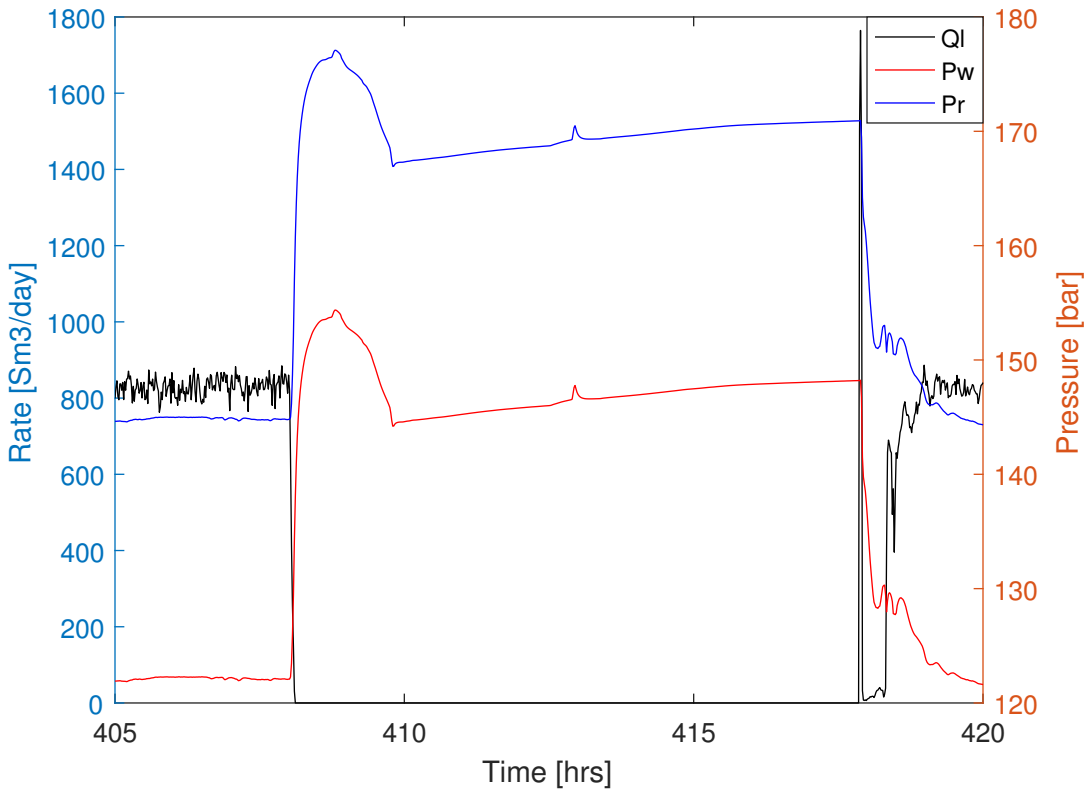

Figure 7.7: Shut-in period to determine the reservoir pressure

7.3 Frequency Analysis

A frequency analysis is used to determine whether the liquid flow rate in November-February in Figure 7.1 and 7.2 has stable oscillations or not. When evaluating an oscillating curve or a periodic behaviour, it is reasonable to use Fourier transform. The Fourier transform converts the data from time domain into frequency domain (Kreyszig, 2011). In Matlab, the discrete Fourier transform can be computed by using the fft-function (fast Fourier transform). Since the sampling rate is 1 measurement per minute, the Nyquist criterion states that larger frequencies than $f_s/2 = \frac{1/\text{min}}{2} = 0.5/\text{min} = 30/\text{hr}$ will not be identified (Wikipedia, 2016).

If there exist a dominating frequency in the frequency spectre, this will be the systems instability frequency and the inverse will tell how long the instability period will last. There can also be other periodical instabilities that will show up as peeks in the frequency spectre. Noise will show up as minor frequencies.

7.3.1 Periods with Noise

Two time intervals in Figure 7.2, respectively January and February 2017 ($t \in (0, 408),\ (895, 1173)$ hrs), and a period in December 2016 ($t \in (705, 1135)$ hrs) in Figure 7.1 have their frequency spectre plotted in Figure 7.8 in blue, red and green colour. These periods does not show any dominating frequency, the frequencies appears as noise. Therefore, one can conclude that the periods act dynamically stable.

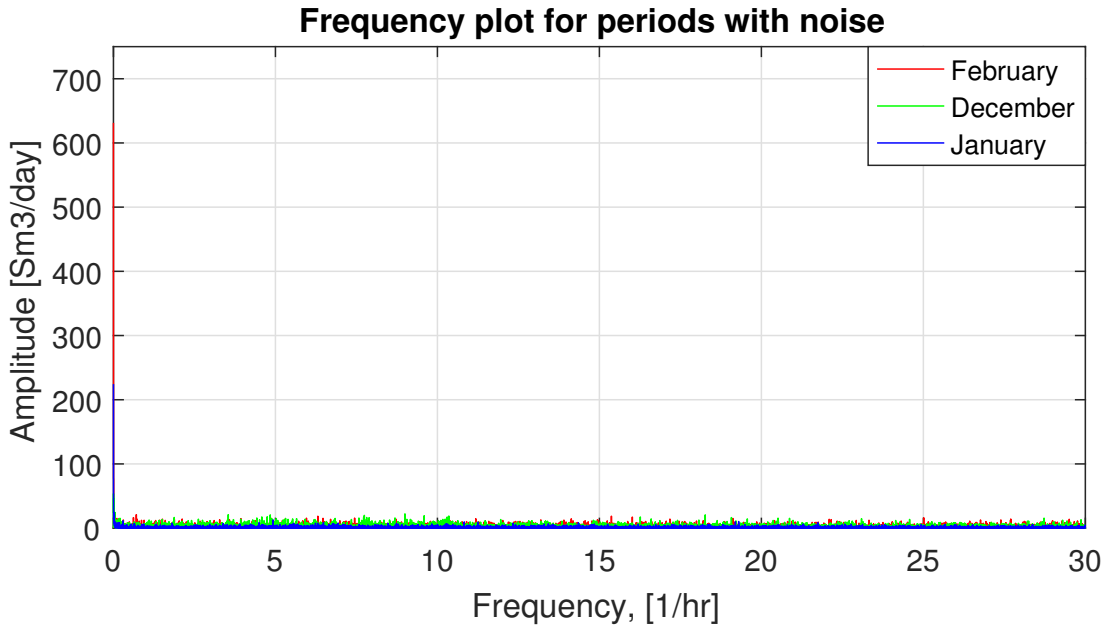

Figure 7.8: Frequency spectre of three stable periods with noise.
There is no clear natural frequency, only noise.

7.3.2 Highly Oscillating Periods

A frequency plot of two highly oscillating time intervals in Figure 7.1, respectively November and December 2016 ($t \in (164, 323),\ (1157, 1159)$ hrs), and a period in January 2017 ($t \in (447, 473)$ hrs) from Figure 7.2 is found in Figure 7.9. These periods with a highly oscillating rate have a clearly dominating amplitude and frequency. January, in blue, has a dominating frequency of $6.4\ \text{hrs}^{-1}$ and the period repeats itself every 9.4 min. November in red and December in green have a quite similar frequency and period.

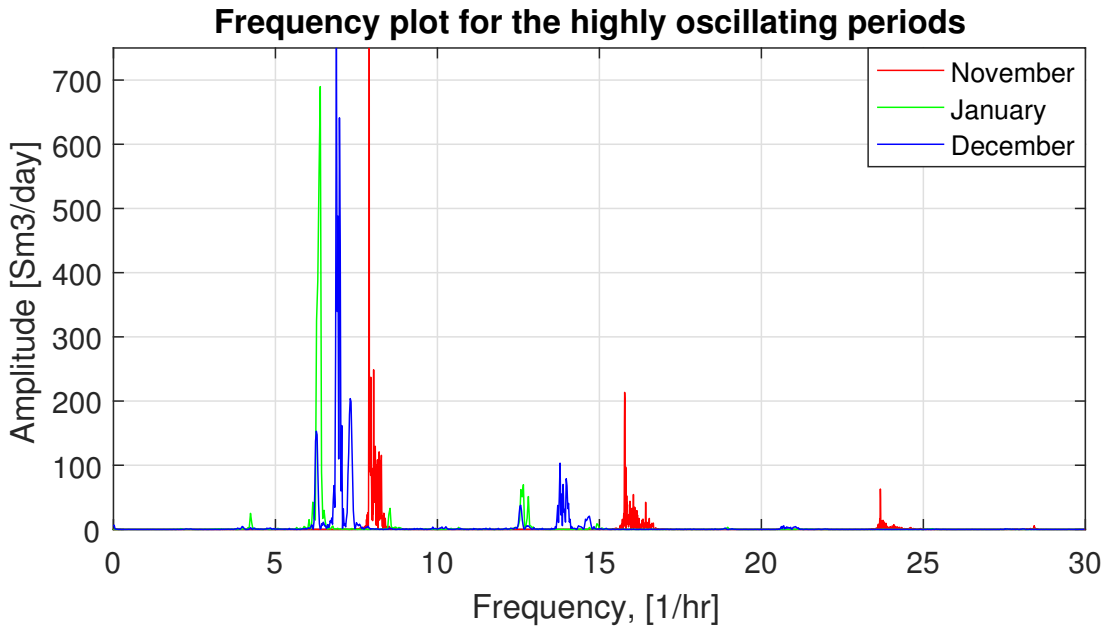

Figure 7.9: Frequency spectre of three highly oscillating periods.
The three periods have a natural frequency between $6 - 8\ \mathrm{hr}^{-1}$

7.3.3 Corresponding Frequency for Other Variables

One can see the same pattern for other variables than the liquid rate in the periods with noise and oscillations. The frequency spectre of the well pressure and the total gas rate are displayed in Figure 7.3.3 and 7.11. The well pressure is plotted in blue and the corresponding y-axis is the one in blue to the left. The gas pressure is plotted in orange and the y-axis to the right in orange applies for the gas rate. The colour codes applies for both Figure 7.3.3 and 7.11.

There is no clear natural frequency of any of the variables in Figure 7.3.3, which corresponds to the interpretation of Figure 7.8. On the other hand, both the well pressure and the gas rate in the unstable periods has approximately the same natural frequency and period as the liquid rate has in Figure 7.9, where the liquid rate in January is plotted in blue.

Highly oscillating time intervals have already been identified in Figure 7.1 and 7.2, several others can be found in Appendix A. The liquid rate, total gas rate and well pressure oscillates with the same frequency in each of the unstable periods. The natural frequencies of the three variables are $5.7 - 7.9\ \mathrm{hrs}^{-1}$ with a corresponding period of $7.6 - 10.6\ \mathrm{min}$ in each unstable period.

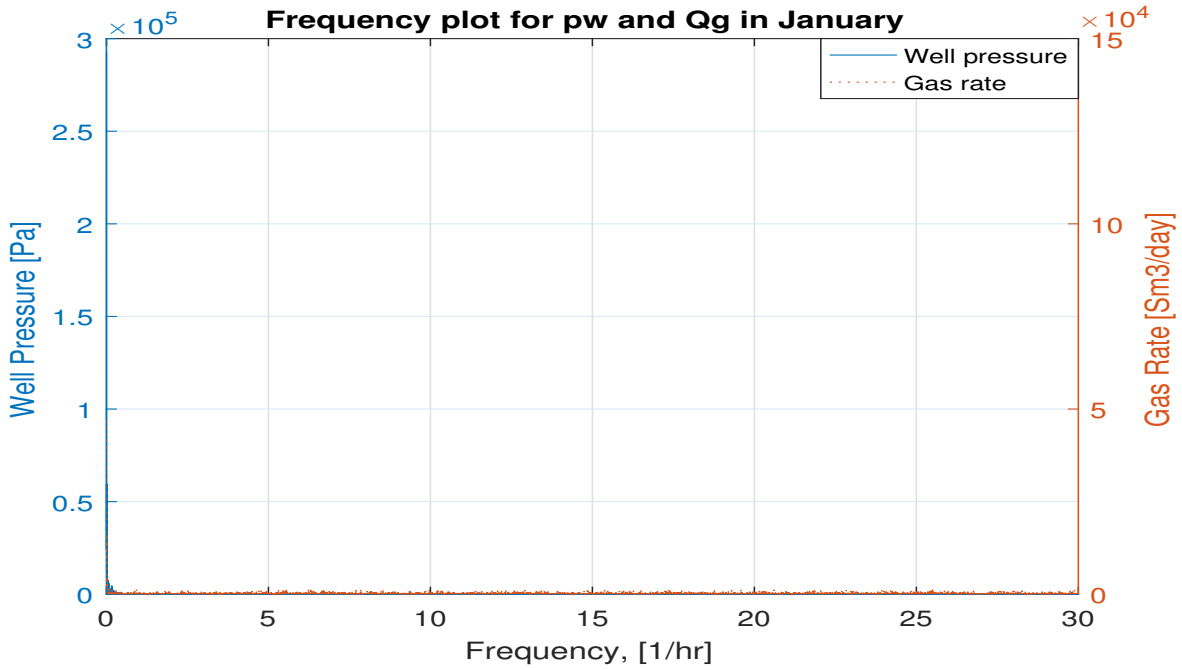

Figure 7.10: Frequency spectre of the well pressure and gas rate for the first 400 hrs in January. There is no clear natural frequency.

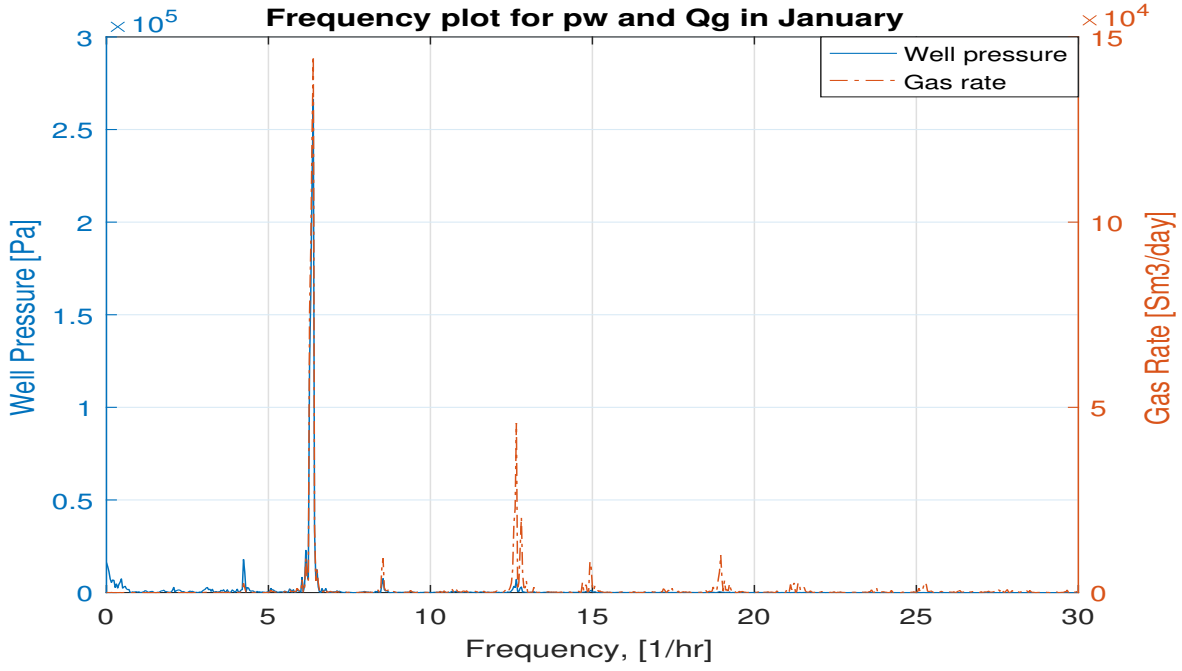

Figure 7.11: Frequency spectre of the well pressure and gas rate in a highly oscillating period in January.

Chapter 8

Results

The results from the stationary and the dynamical model are presented in this chapter. Data from well A-23 at Heidrun were used as input. A pressure response analysis is also performed and presented.

8.1 Stationary Model

8.1.1 Comparing the Model with Several Periods

Data from several periods between January 1st 2016 and February 22nd 2017 are used to evaluate the stationary model for accuracy of the pressure estimation. The production between January 1st to October 31st 2016 can be seen in Appendix A, while November 1st 2016 to February 22nd 2017 can be seen in Figure 7.1 and 7.2 in Chapter 7.1.1.

Pressure and rates for a stationary case are estimated by averaging the pressure and rate data for the particular periods, as were done for the period in $t \in (0, 408)$ hrs in January 2017 seen in Table 4.1 in Chapter 4.7. The averaged values for the tubing pressure are displayed in Table 8.1. The periods are divided into two groups, characteristics of low and high amplitude. The periods in the low amplitude specter are the periods that are characterized by noise and a non existing natural frequency. The periods in the high amplitude group are the highly oscillating periods.

The value of the drift velocity were set to be equal to the one in Chapter 4.7, that is $v_o = 0.2\ \mathrm{m/s}$. For the periods with a standard deviation less than $600\ \mathrm{m^3/day}$, the gas distribution factor are $C_o = 1.30$. This concerns all the periods with low amplitude and the period in February 2016 in the high amplitude group. The range for the periods with a high amplitude, except for February 2016, is $C_o = 1.36 - 1.60$ for a rate deviation of approximately $830 - 1400\ \mathrm{Sm^3/day}$.

The error of the pressure estimation at the gauge carrier is displayed in the column to the left in Table 8.1. The error ranges from $-2.3\ \%$ to $1.2\ \%$. However, it is only two periods with an error greater than $\pm 0.8\ \%$.

Table 8.1: Comparison of the Measured and Estimated p_t at the gauge carrier depth

Amplitude	Period	Time [hrs]	Measured $\overline{p}_t$ [bar]	Calculated p_t [bar]	Error [%]
	March	$t = 48 - 413$	128.55	129.32	-0.601
	November	$t = 582 - 705$	119.61	119.02	0.496
	December	$t = 705 - 1131$	119.61	118.59	0.219
Low	January 2017	$t = 0 - 408$	122.49	122.73	-0.195
	February 2017	$t = 895 - 1173$	122.57	122.89	-0.264
	February	$t = 1002 - 1153$	128.73	129.75	-0.791
	March-April	$t = 562 - 1153$	124.98	127.91	-2.343
	May	$t = 220 - 430$	120.22	120.48	-0.220
High	October	$t = 758 - 1100$	118.18	116.74	1.213
	November	$t = 164 - 323$	116.28	116.81	-0.456
	December	$t = 1157 - 1199$	119.27	119.19	0.066
	January 2017	$t = 447 - 473$	120.43	120.07	0.299

8.1.2 Stability Analysis

The stability analysis for January 2017 is presented in this chapter. Figure 7.2 of January 2017 in Chapter 7.1.1 shows the general behaviour with oscillations with both high and low amplitude.

The pressure response plots in Figure 8.1 illustrates how the pressure develops when the pressure experiences an initial disturbance. The pressure at the bottom of the well is plotted in blue and the annular pressure is in orange. Equation 6.2 in Chapter 6, which does not account for the outlet, is used to create the top plot in Figure 8.1. The differential Equation 6.1, which accounts for the inflow and outflow, is used for the bottom plot in Figure 8.1.

An initial disturbance of $\delta p_{wf} = 1$ Pa and $\delta p_g = -1$ Pa are applied and how the pressure responds is evaluated. If the disturbance leads to increasing oscillations with time, the system will appear dynamically unstable. If the oscillations dies out, one can assume that the well will be stable.

The frequency analysis in Chapter 7.3 declared that the period $t \in (0, 400)$ hrs in January 2017 was a stable period that experiences noise. Figure 8.1 illustrates the pressure response for this period. The top plot, which does not consider time delay, shows damped oscillations and therefore a stable behaviour. The well uses 30 min from the pressure disturbance is applied until the well has reached the initial state. When considering the outflow, seen in the bottom plot, the pressure oscillates, however, the signal does decrease in amplitude for each wavelength. The oscillations dies out after 180 min. This means that the dynamical response is damped and the well will appear stable.

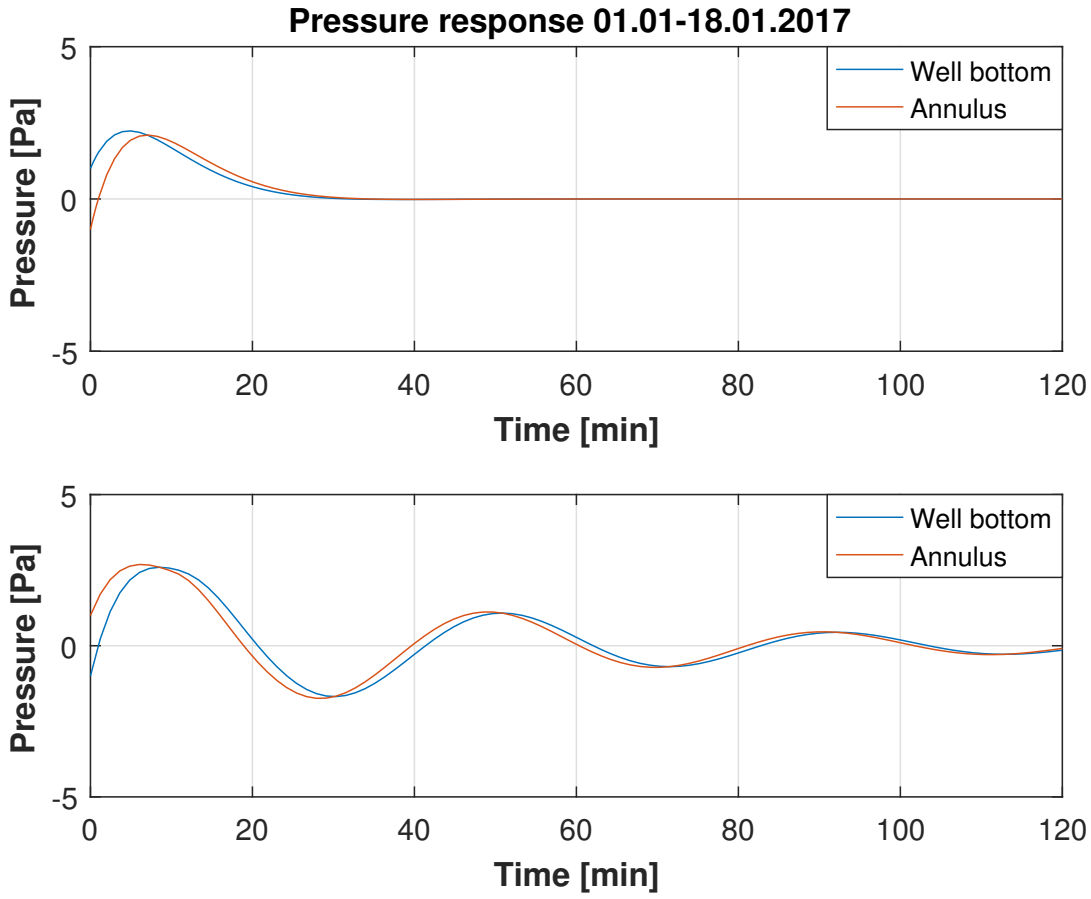

Figure 8.1: Dynamical response at the beginning of January 2017 at Heidrun. The pressure response is damped and, therefore, indicates a stable well.

Table 8.2 consist of all the periods as seen organized in Table 8.1. Table 8.2 displays the time delay, Δt, between inflow and outflow and how long time it takes before the pressure has returned to its initial state. One important thing to notice is that all of the periods shows damped oscillations and a stable well, even though the analysis in Chapter 7.3 shows signs of instabilities.

Table 8.2: Pressure Response

Amplitude	Period	Time [hrs]	Δt [min]	Returned to initial state [min]
Low	March	$t = 48 - 413$	10.26	150
	November	$t = 582 - 705$	8.92	140
	December	$t = 705 - 1131$	8.86	140
	January 2017	$t = 0 - 408$	10.47	180
	February 2017	$t = 895 - 1173$	9.85	140
High	February	$t = 1002 - 1153$	9.68	120
	March-April	$t = 562 - 1153$	8.27	120
	May	$t = 220 - 430$	5.43	80
	October	$t = 758 - 1100$	8.09	120
	November	$t = 164 - 323$	4.58	80
	December	$t = 1157 - 1199$	6.87	100
	January 2017	$t = 447 - 473$	8.05	120

8.2 Dynamical Model

The period in January 1st to 18th and the highly oscillating period between January 19th and 20th in Figure 7.1 will be used to demonstrate and evaluate the dynamical model for a time period of $8\ \mathrm{hrs}$.

The pressure plots in the following sections are all build up in the same way. The estimated well-head pressure is plotted in green, the pressure at the injection point in black, the pressure at the gauge carrier in blue and the bottomhole pressure in magenta. The measured wellhead pressure is the dotted green curve and the measured downhole pressure is plotted in a dotted blue line.

The pressure in the tubing at the injection point is estimated from the choke flow relationship, while the other pressure estimations are based on integrating the pressure drop along the tubing .

8.2.1 Flow Rate Data with Time Delay

Highly Oscillating Period

The highly oscillating period is simulated in Figure 8.2, 8.3 and 8.4. Figure 8.2 displays the well pressure at different depths. The time for the fluid to propagate from bottomhole to the wellhead was considered, and it was estimated to be $\Delta t \approx 9$ min. Between the bottomhole and the gauge carrier the time delay is $\Delta t \approx 2$ min. The estimated pressures seems to follow the trend of the measured pressures, however, this is easier to see in Figure 8.3.

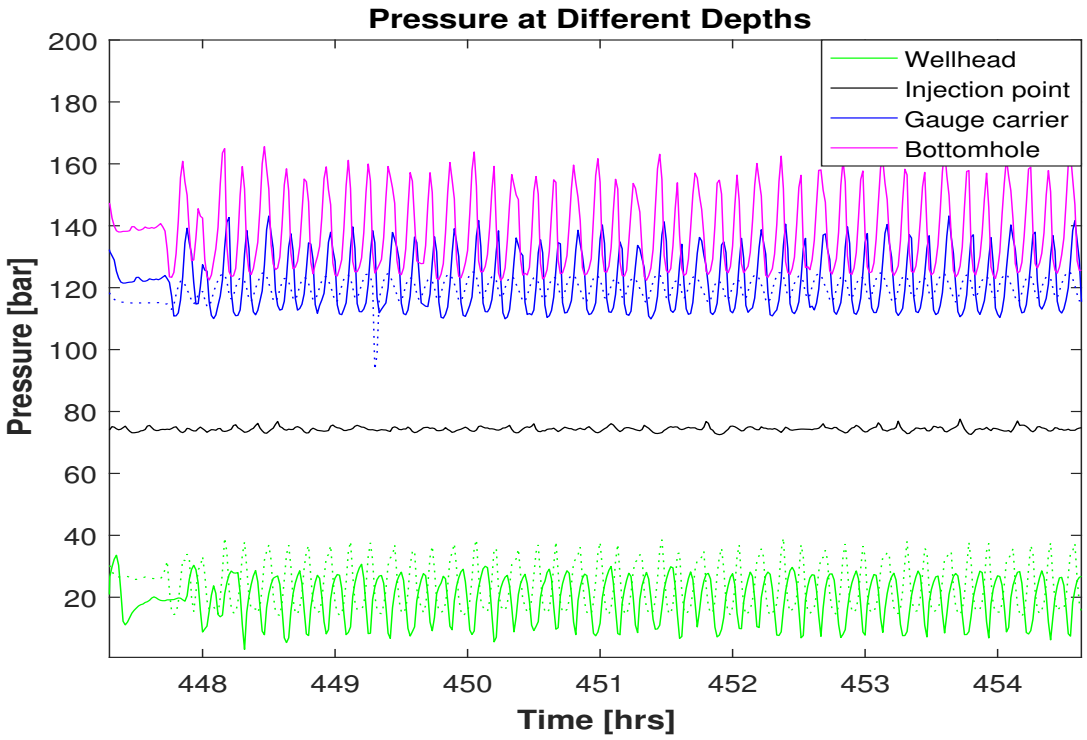

Figure 8.2: Estimated and measured pressure at different depths based on the flow rate data for a highly oscillating period in January.

Figure 8.3 displays the oscillations of the estimated and measured pressures clearer. The green curve is the wellhead pressure and the corresponding measured wellhead pressure is plotted in a green dotted line. The pressure at the gauge carrier is in blue, as well as the measured pressure downhole which is the blue dotted line.

The well pressure at the point of the downhole pressure measurement has a higher amplitude in the oscillations than the measured pressure at the same point in Figure 8.3. The amplitude of the oscillations in the wellhead pressures are approximately the same. However, the estimated and measured pressure oscillates with a phase delay in the period, because the propagation time is accounted for.

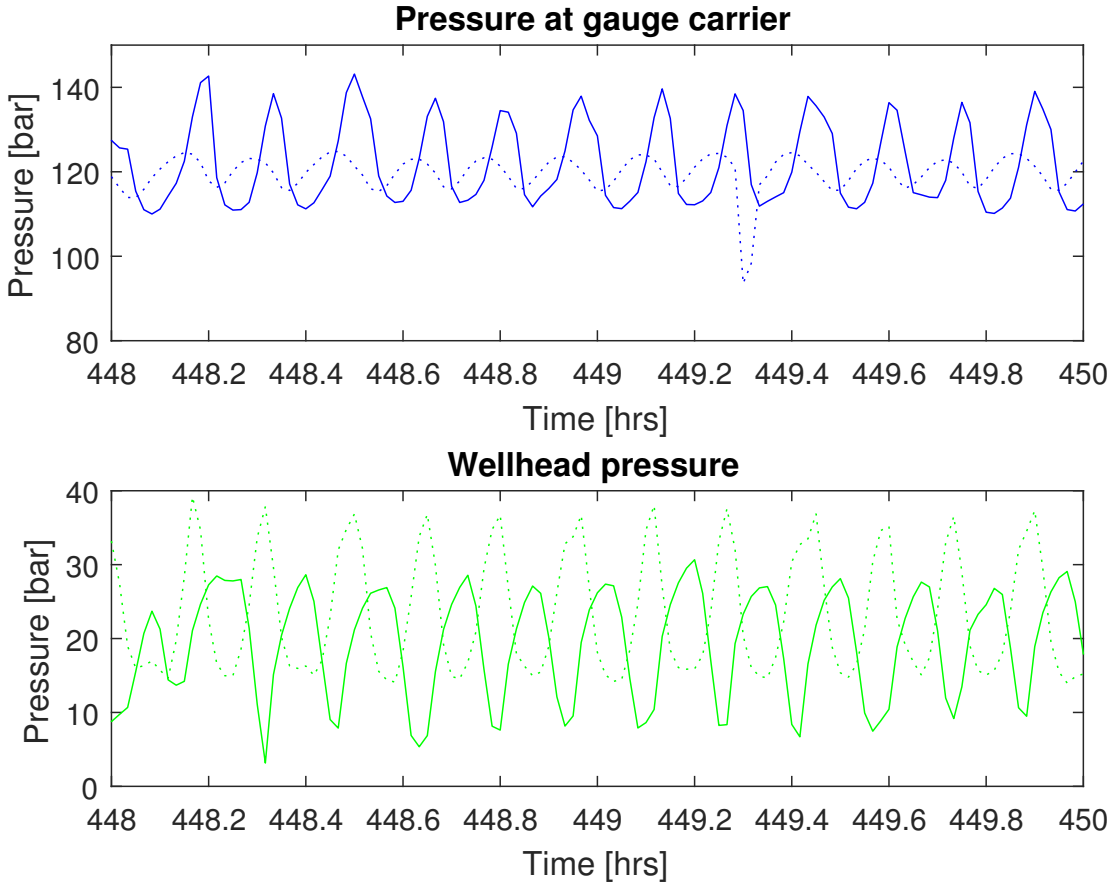

Figure 8.3: Estimated and measured tubing and wellhead pressure at different depths for a highly oscillating period in January.

The exponential moving mean over 10 data points were used to estimate the flow rate. This was done to account for the uncertainty in the multiphase flow measurement. Another reason was that the model handled the extreme high and lows poorly. Since the real flow rate data were used, the estimated and measured flow rate corresponds to a certain extent in Figure 8.4.

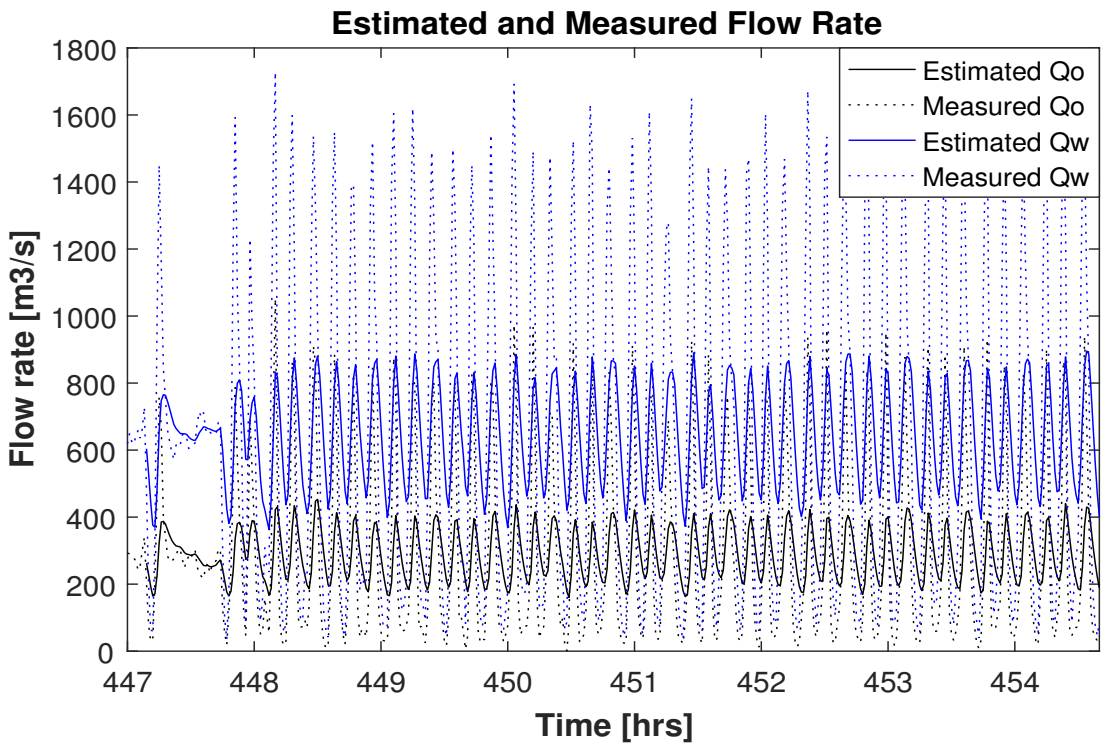

Figure 8.4: Estimated and measured flow rate for a highly oscillating period in January.

8.2.2 Inflow Performance Relationship

Stable Period

Figure 8.5 illustrates the well pressure at different key depths. The simulated wellhead pressure is plotted in green and the measured wellhead pressure is plotted in a green dotted line. The average error between the estimated and measured wellhead pressure is approximately $29.7\ \%$.

The blue line in Figure 8.5 is the estimated tubing pressure at the pressure measurement depth. The actual well pressure measurement is the dotted blue curve. The mean error is roughly $9.1\ \%$ between the estimated and measured tubing pressure.

Figure 8.6 illustrates the estimated oil rate and water rate in black and blue, respectively. The dashed lines in black and blue represents the measured oil rate and water rate. It is very clear from the graph that the estimated rates does not correspond with the measured ones.

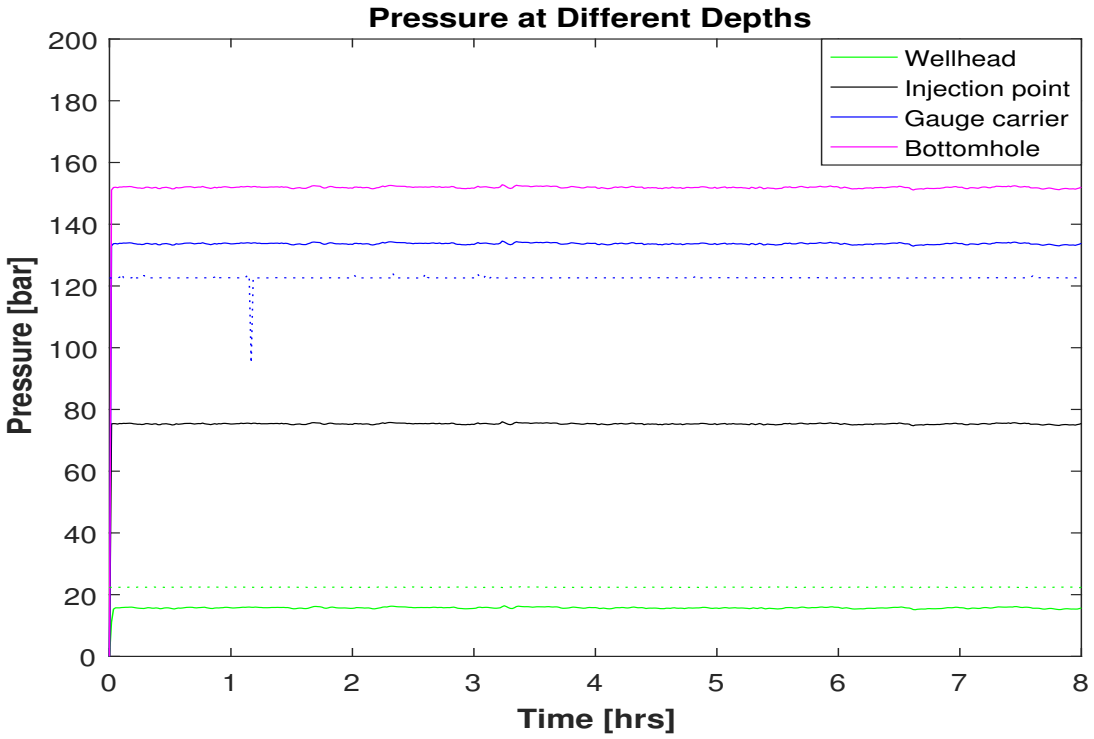

Figure 8.5: Estimated and measured pressure based on an inflow performance relationship at different depths for a stable period in January.

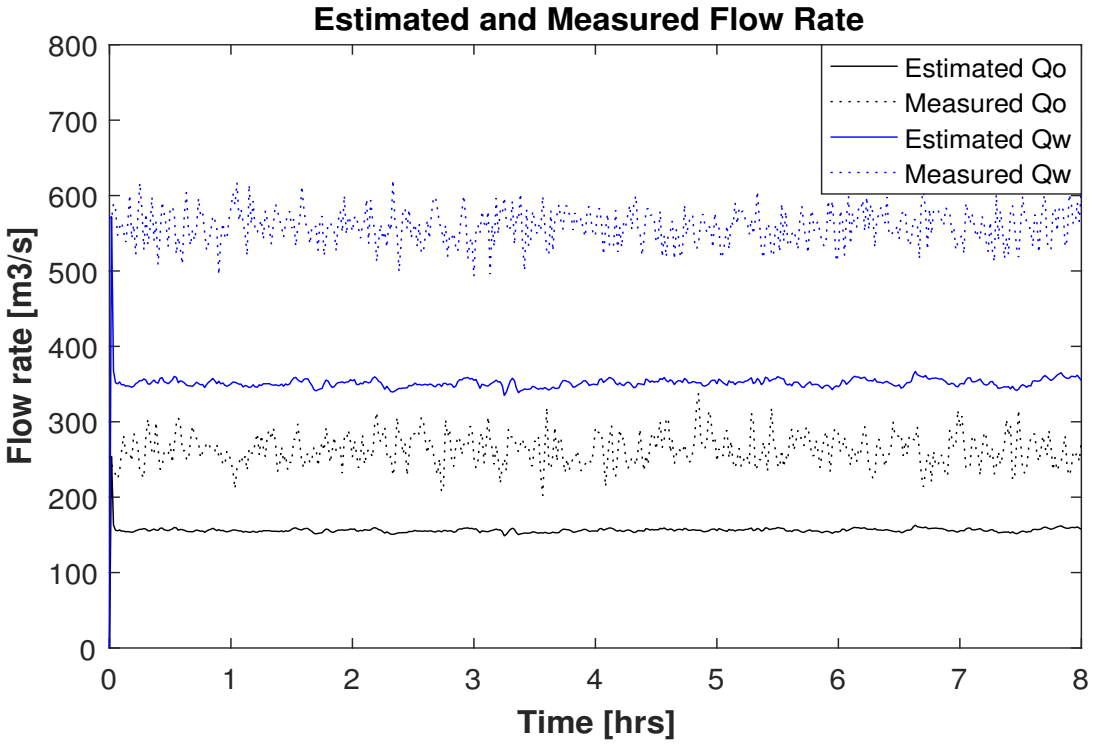

Figure 8.6: Estimated and measured flow rate based on an IPR for a stable period in January.

Highly Oscillating Periods

Figure 8.7 and 8.9 illustrates exactly the same as Figure 8.5 and 8.6, however, the data used are from the highly oscillating period in January 19^{th} to 20^{th}. The error is $29.7\ \%$ for the estimated wellhead pressure and $2.7\ \%$ for the estimated pressure at the gauge carrier, seen in Figure 8.7.

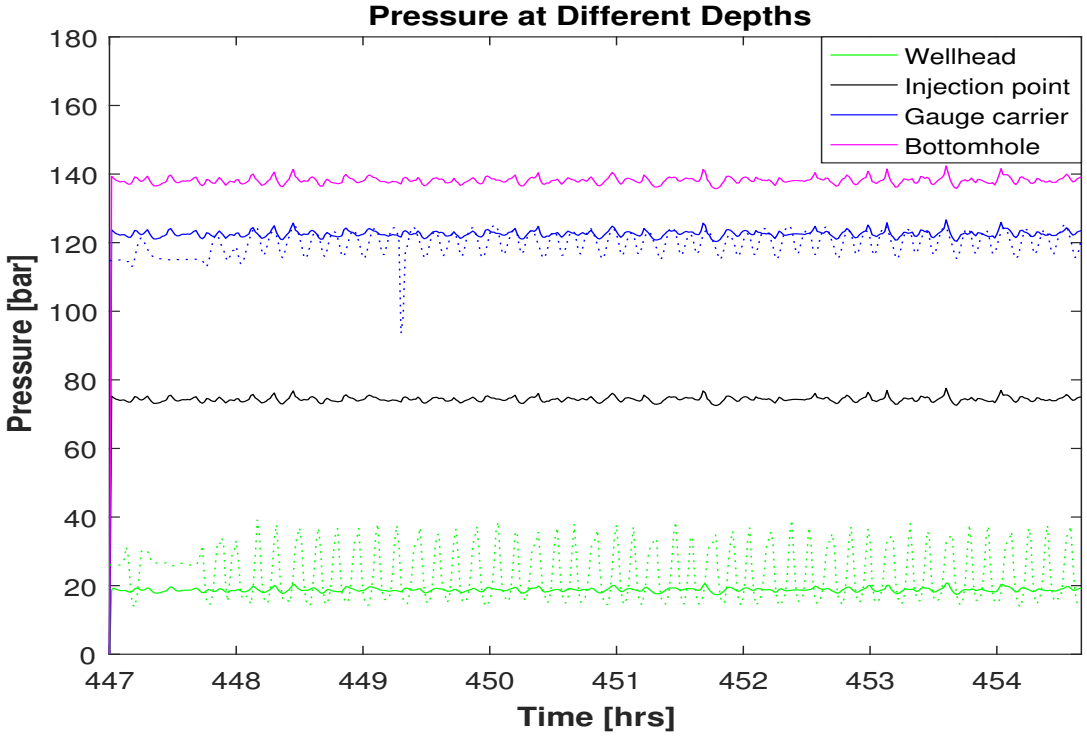

Figure 8.7: Estimated and measured pressure based on an IPR at different depths in a highly oscillating period in January.

Figure 8.8 illustrates the difference in the oscillations in the estimated and measured pressure at the gauge carrier and at the wellhead. The estimated oscillating pressures has a much smaller amplitude than the measured ones.

The estimated flow rates in Figure 8.9 do not compare with the measured ones. The estimated flow rates do not oscillate with a certain frequency and period, the signal is more characterized by random fluctuations. The mean value of the measured flow rates are $289\ \mathrm{Sm}^3/\mathrm{day}$ and $641\ \mathrm{Sm}^3/\mathrm{day}$. This is approximately the same as the mean values of the estimated flow rates.

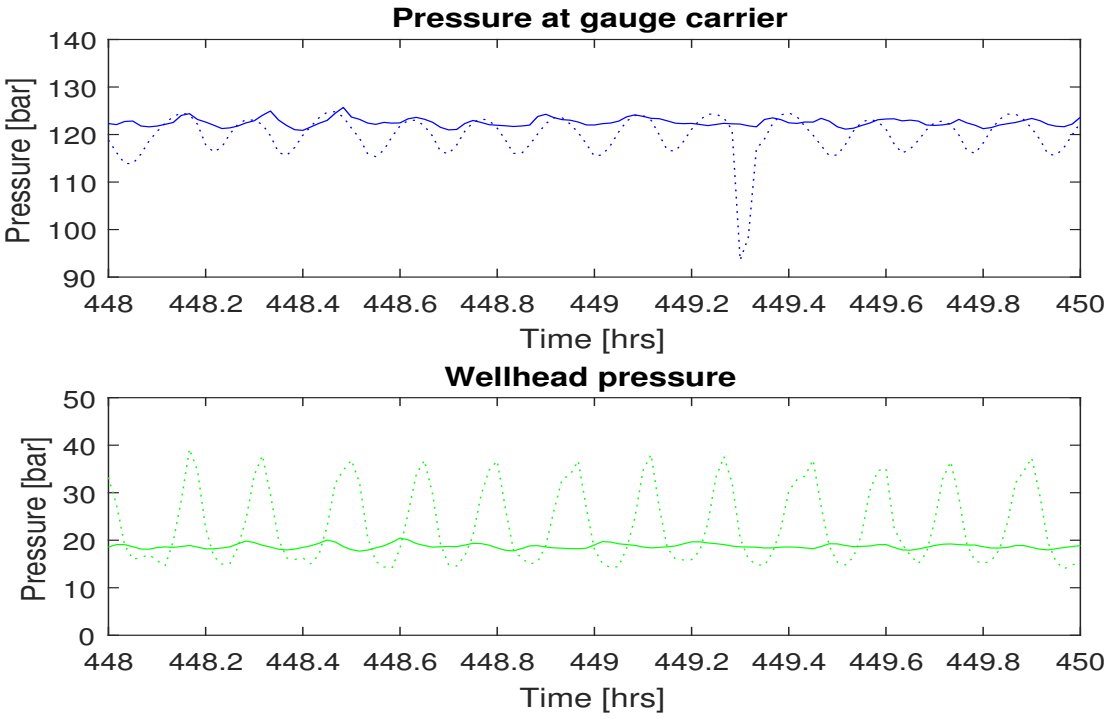

Figure 8.8: Estimated and measured tubing and wellhead pressure based on an IPR at different depths for a highly oscillating period in January.

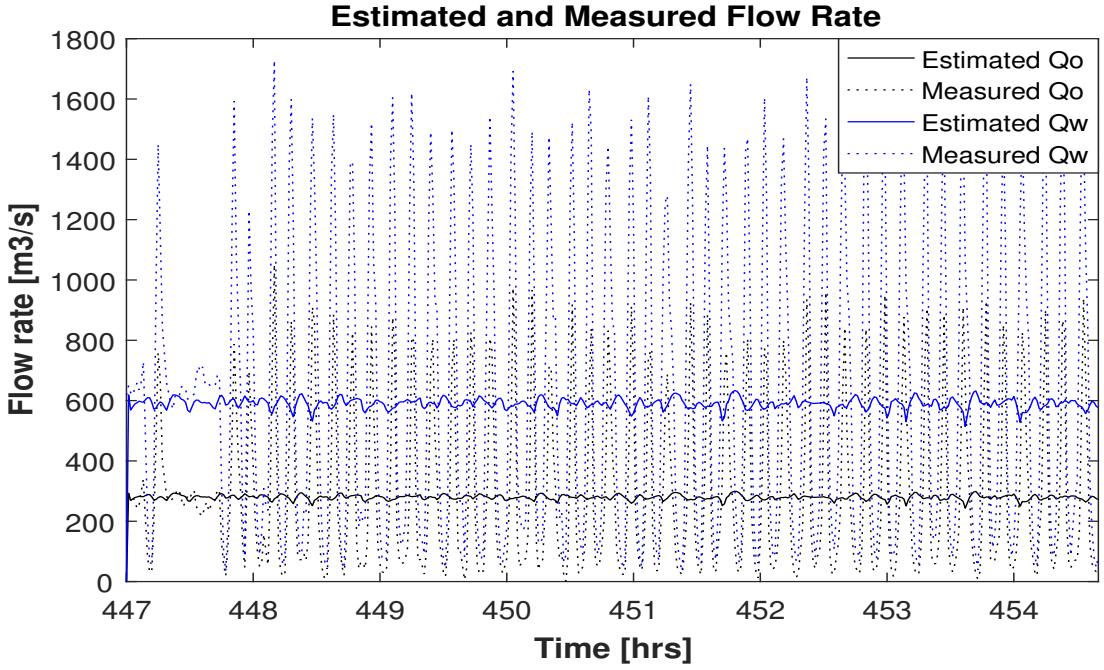

Figure 8.9: Estimated and measured flow rate based on an IPR in a highly oscillating period in January.

Chapter 9

Discussion

9.1 Dynamical Well Behaviour

The analysis of the dynamical well behavior presented in Chapter 7 showed that there exists mainly two types of production profiles in well A-23. One of them are characterized by a steady production with evenly distributed noise, and the other by frequency dominated oscillations.

There were no clear signs of why the production suddenly changes from stable to highly oscillating.

Since the gas lift pressure and lift-gas rate were constant even though the production changed back and forth from stable to oscillating, it can be assumed that the annulus does not respond to tubing variations.

9.2 Downhole Gas Injection Valve Performance

The given downhole gas injection orifice port size was used in the stationary model in Chapter 4. However, when comparing the estimated pressure in the tubing and in the annulus at the injection point, they did not satisfy the choke flow relationship.

It is very unlikely that the pressure estimation down the tubing is the reason for the differential pressure inconsistency across the downhole injection valve. If this were the case, the pressure

profile would have had a more gentle slope from the wellhead and down to the injection valve and then a pressure reduction down to the gauge carrier. There is no natural reason for the well pressure to decline.

An excessively high estimate of the annular pressure at the gas injection point could also have led to the inconsistency. However, the gas lift pressure at the wellhead is approximately $119\ \mathrm{bar}$, which means that the pressure gradient must be negative to be able to obtain a pressure differential of $7.3\ \mathrm{bar}$ across the downhole orifice. Again, this is not possible.

The choke flow equation is derived in Appendix B. During the derivation, some assumptions were taken, including an equal cross-sectional area of the tubing and annulus. However, the difference in the actual cross-sectional areas are $\Delta A = A_t - A_a = 0.0116 - 0.0047 = 0.0069\ \mathrm{m}^2$. Thus, the tubing cross-sectional area is over twice as large as the annular. This assumption in addition to the assumption about a slightly compressible gas makes the choke flow relationship in Equation 4.18 questionable. Other correlations can be considered, like Thornill-Craver equation for gas flow rate through an orifice (Winkler and Blann, 2007:p. 538). However, other equations are also based on assumptions or on variables that cannot be obtained for this assignment.

In this thesis it was assumed that both the choke flow equation and the tubing and annular pressure estimations were valid. In result, the size of the downhole injection orifice port size was changed to satisfy the choke flow relationship. As a result, the tubing pressure could be estimated from the annular pressure and the inflow from the reservoir in the dynamical model.

9.3 Multiphase Flow Meter

The multiphase flow measurement is not as accurate as a single phase flow meter. In addition, the multiphase flow measurements represents the outflow. If the flow is stationary, inflow and outflow will be the same. However, if the flow rate in the outlet varies, then the inflow must vary too. Because the flow propagates with the kinematic velocity up the tubing, there will be a latency between the variables in the inlet and outlet. If the outflow rate is averaged over a greater interval than one oscillation period, then this number can represent the inflow rate.

The stationary model in Chapter 4 is based on the mean value of the flow rate data. This is a good estimate for the stable periods that shows noise in the measurements. The standard deviation is small and the data is distributed normally around the average value. Thus, it may be reasonable to use the average of the variables. However, in the highly oscillating periods the average value does not capture the characteristic oscillating behaviour.

9.4 Production Choke

At well A-23 at the Heidrun field, Statoil is using a production choke to throttle the outflow. The choke opening is held constant for the most part, but it has been adjusted occasionally, mainly to close it during the shut-in periods. The choke opening size has not been considered in the models, even though throttling of the production may lead to noise and oscillations seen in the multiphase flow measurements.

The size of both the production and gas lift choke opening was inspected to see if it had an effect on the beginning or end of the oscillating periods in the transition between the production periods in Chapter 7.1.3. The choke openings were kept constant during this period and did therefore not have any effect on the fluctuations.

9.5 Stationary Model

The reliability check in Chapter 8.1.1 showed promising results. The highest difference in pressure was $2.93\ \mathrm{Pa}$, which is an error of $2.3\ \%$.

Even though the error of the model is small, the estimation at the gas injection valve for the tubing pressure and for the annular pressure does not correspond with each other according to the choke flow relationship. This has been addressed in Section 9.2.

The pressure response analysis indicates that all of the tested periods are stable. Even though some of the periods experiences stochastic noise or extreme oscillations. The input in the pressure

response analysis is based on an initial condition from a linearization of the data. This should be able to give an accurate estimate of the stability.

One of the reasons the response analysis can show a stable well when other measures tells that it is in fact unstable, is that the analysis shows that it will take over $80\ \mathrm{min}$ for each of the period to return to the initial state. However, if another disturbance occurs before this time has past, the well will not be able to reach the stable initial conditions and it will appear as unstable. Another reason is that one of the assumption in the differential equation from Chapter 6 is a connection between the tubing and annulus. However, the concept behind the instabilities occurring is not casing heading, because the annular variables are unaffected by the variations in flow rates and pressure in the tubing.

9.6 Dynamical Model

Because of the time delay between inflow and outflow, it is not possible to use the multiphase measurements of the flow rate taken at the outlet with the well pressure taken at the gauge carrier at the same time, since they do not correspond. The fluid at the point of the bottomhole pressure measurement uses Δt time before it reaches the multiphase flow measurement. Before one specific measurement of the flow rate can be used, the time delay or must be accounted for. This was not necessary for the stationary model, since it linearization of the variables.

Instead of adding the phase delay to the measurements, a correlation based on the inflow performance can be used. This means that there are only a need for the measurements taken at the gas lift choke, that is the gas lift pressure and the lift-gas flow rate.

9.6.1 Flow Rate Data with Time Delay

By using the flow rate data and account for the propagation time in the tubing a good estimation for flow rates and well pressures were accomplished.

An exponential moving average over 10 data points were used to estimate the flow rates, because

of the uncertainties in the measurements. The number of data points were chosen arbitrary.

The pressure estimation follows the trend in the highly oscillating periods simulated in Chapter 8.2.1. There is a phase delay between the estimated and measured pressures, this is seen in Figure 8.3. The reason for this is that the propagation time is accounted for in the estimated pressure, while the pressure measurement does not consider it.

Even though this model estimates the pressures precisely, it is not optimal. The reason is that the pressure is based on flow rate measurements. The model can no longer be used to predict the flow rate or well performance when changing the gas lift measurements, because the measured flow rate is needed.

9.6.2 Inflow Performance Relationship

The advantage of the flow rate estimation is that there is no need for flow rate measurements, only one initial measurement to determine the productivity index.

The oil and water rate does not correlate with the measured rates in Chapter 8.2.2. Regarding the simulation of the highly oscillating period, the mean value of the estimated flow rate matched the measured one, however, the estimated flow rate did not capture the oscillating behaviour. A certain amount of deviation is expected since the multiphase measurements are somewhat inaccurate. However, according to the stable simulation, the multiphase measurements must have overestimated the rates by $36 - 40\ \%$. This is not very likely, thus, the inflow relationship used in this model cannot be valid.

Another approach than the standard inflow performance relationship should be considered to estimate the inflow. Wiggins (1993) presented an inflow performance relationship based on three-phase flow and Asheim (2000) related the inflow to the dynamical behaviour. Chapter 7.3 showed that the flow rate oscillated with a certain frequency in the periods with a high amplitude, this can be related to the inflow performance.

Since the flow rate estimations were inaccurate, it follows that the pressure estimation will not be that precise either, because the pressure is a function of flow rate.

When adjusting the gas distribution factor to optimize the bottomhole pressure estimation in the highly oscillating periods a dependency between this factor and the flow rate was discovered. However, if the gas distribution factor would change with the flow rate, it would exceeds its validity range. Nevertheless, this detail adds on to the limitations of the model.

9.7 Recommendations for Further Work

Some simplifications were done during the implementation of the models, like the gas viscosity guess, the oil viscosity as a function of pressure only and neglecting the water volume factor. However, these parameters have a very small effect on the result.

For further studies it is recommended to:

- Verify the large pressure drop between the tubing and annulus across the downhole injection valve. Is this because the given downhole injection valve size is wrong or does the choke flow relationship underestimate the pressure differential.
- Investigate the effect the production choke has on the oscillations. This was only explored for one transition period in this thesis.
- Since the oscillating behaviour is a result of the inflow dynamics, another inflow correlation that captures the dynamical inflow behaviour would improve the dynamical model. A suggestion of another inflow correlation is to use a dynamic productivity index as a function of the oscillating amplitude.

Chapter 10

Conclusion

Adequate measurements of the flow rates and pressures at different locations in well A-23 at Heidrun have been analyzed. To gain quantitative insight, models have been implemented to attempt predictions of the observed behaviour.

To implement the measurements, a stationary gas lift model was developed. The model estimated the well pressure within an error of $2.3\ \%$ compared to the measured pressure.

Analyzes showed that during dynamically stable periods, the well was subjected to rate variations around $7\ \%$. These were stochastic and normally distributed.

During the unstable periods, the flow rates oscillated with amplitude around $90\ \%$ and a period of $7-10\ \mathrm{min}$. There were no clear preliminary reason for the sudden change from a steady production to the highly oscillating behaviour, based on the measurements.

A dynamical model to simulate the well pressure was developed. The predictions was not consistent with the oscillations observed from the measurements, because the inflow correlation did not compare with the measured data.

The pressure response analysis did not show any sign of instabilities. The likely reason is that the large pressure drop across the downhole injection valve makes gas inflow independent of tubing pressure variation, this prevents casing heading which was assumed by the model. As a result, casing heading cannot be the reason for the oscillating production.

List of Symbols

The next list describes the symbols that are used within this thesis

A	Cross-sectional area	m^2
a	Blick et al. (1988) constant	$1/\mathrm{hr}$
$a_w,\ a_g$	Inflow coefficients	$1/\mathrm{s}$
B	Formation volume factor	$\mathrm{m}^3/\mathrm{Sm}^3$
b	Blick et al. (1988) constant	
c	Inflow/outflow coefficients	$1/\mathrm{s}$
c_f	compressibility	$1/\mathrm{Pa}$
C_S	Wellbore storage constant	m^3/Pa
C_T	Tubing capacitance	m^3/Pa
$d_w,\ d_g$	Outflow coefficients	$1/\mathrm{s}$
E	Downhole injection valve efficiency factor, assumed to be 0.9	
f	Friction	
$F_{1,\,2}$	Stability criteria	
F_c	Parameter group	
g	Acceleration of gravity	m/s^2
ID	Inner diameter	m
ID_{valve}	Downhole injection valve port size	m
J	Productivity index	$\mathrm{Sm}^3/\mathrm{Pa}/\mathrm{s}$

$K_1,\ K_2,\ K_3$	Blick et al. (1988) characteristic equation coefficients	
L	Length	m
M	Gas molecular weight	g/mol
$M_1,\ M_2$	Tubing inertance	$\mathrm{Pa} \cdot \mathrm{s}^2/\mathrm{m}^3$
n	Amount of gas	mol
OD	Outer diameter	m
p	Pressure	Pa
p_m	Constant pressure at the gas injection manifold	Pa
Q	Rate	m^3/s
R	Universal gas constant	$\mathrm{m}^3\mathrm{Pa/k/mol}$
r	Gas-oil-ratio of the inflow	
R_s	Gas solubility in oil	$\mathrm{Sm}^3/\mathrm{Sm}^3$
r_w	Wellbore radius	m
r_{ch}	Ratio of casing pressure and p_m	
r_{eD}	Dimensionless reservoir diameter	
r_v	Ratio of tubing and casing pressure	
Re	Reynolds number	
T	Temperature	K
t	Time	s
$t + \Delta t$	Time lag	s
t_D	Dimensionless time	
V	Volume	m^3
z	Gas compressibility factor	

Greek Symbols

α	Real part of eigenvalues	$1/\mathrm{s}$
$\Delta\rho$	Density difference between oil and lift-gas	kg/m^3
Δp	Pressure drop in tubing	Pa

δ	Dynamic disturbance	
γ	Specific gravity	$\mathrm{m}^3/\mathrm{Sm}^3$
$\lambda_1,\ \lambda_2$	Eigenvalues	
μ	Viscosity	$\mathrm{Pa}\cdot\mathrm{s}$
μ_{ch}	Ratio of casing zT and gas injection manifold zT	
μ_v	Ratio of tubing zT and casing zT	
ω	Angular frequency, imaginary part of the eigenvalues	$1/\mathrm{s}$
ϕ	Porosity	
ρ	Density	kg/m^3
σ	Standard deviation	

Subscripts

a	Annulus
c	Kinematic
csg	Casing
g	Gas
i	Injection
l	Liquid
m	Mixture
o	Oil
r	Reservoir
s	Superficial
sc	Standard condition
t	Tubing
th	Tubing head
tp	Two-phase
w	Water
wf	Bottomhole

References

Aguilar, M. L. et al. (2011). “Flow Instabilities in Gas-Lift Wells with Water Coning”. *SPE Middle East Oil and Gas Show and Conference, 25-28 September, Manama, Bahrain. SPE 142694*.

Alhanati, F. J. S. et al. (1993). “Continuous Gas-Lift Instability: Diagnosis, Criteria and Solutions”. *SPE Annual Technical Conference and Exhibition, 3-6 October, Houston, Texas. SPE 26554*.

Asheim, H. A. (1986). “Mona, an Accurate Two-Phase Well Flow Model Based on Phase Slippage”. *SPE 12989*.

Asheim, H. A. (1988). “Criteria for Gas-Lift Stability”. *SPE 16468*.

Asheim, H. A. (1999). “Verification of Transient, Multi-Phase Flow Simulation for Gas Lift Applications”. *SPE Annual Technical Conference and Exhibition, 3-6 October, Houston, Texas. SPE 56659*.

Asheim, H. A. (2000). “Analytical Solution of Dynamic Inflow Performance”. *SPE Annual Technical Conference and Exhibition, 1-4 October, Dallas, Texas. SPE 63307*.

Asheim, H. A. (2016). *Compendium in Production Wells*. Chap. 11. Gas Lift.

Blasius, H. (1913). “Das Ähnlichkeitsgesetz bei Reibungsvorgängen in Flüssigkeiten”. *Mitteilungen über Forschungsarbeiten auf dem Gebiete des Ingenieurwesens*. Springer, pp. 1–41.

Blick, E. F., P. N. Enga, and P. C. Lin (1988). “Theoretical Stability Analysis of Flowing Oil Wells and Gas-Lift Wells”. *SPE 15022*.

Dalsmo, M., E. Halvorsen, and O. Slupphaug (2002). “Active Feedback Control of Unstable Wells at the Brage Field”. *SPE 77650*.

Eikrem, G. O., O. M. Aamo, and B. A. Foss (2006). “Stabilization of Gas-Distribiution Instability in Single-Point Dual Gas Lift Wells”. *SPE 97731*.

Eikrem, G. O., O. M. Aamo, and B. A. Foss (2008). "On Instability in Gas Lift Wells and Schemes for Stabilization by Automatic Control". *SPE 101502*.

Evers, M. G. L., V. L. van Beusekom, and R. A. W. M. Henkes (2009). "Appearance and mitigation of density waves in continuously gas-lifted wells". *14th International Conference on Multiphase Production Technology, 17-19 June, Cannes, France*. BHR-Group.

Fairuzov, Y. V. et al. (2004). "Stability Maps for Continuous Gas-Lift Wells: A New Approach to Solving an Old Problem". *SPE Annual Technical Conference and Exhibition, 26-29 September, Houston, Texas. SPE 90644*.

Fekete-Associates-Inc. (2012). *Average Reservoir Pressure*. URL: http://www.fekete.com/SAN/TheoryAndEquations/WellTestTheoryEquations/Average_Reservoir_Pressure.htm.

Grupping, A.W., C.W.F. Luca, and F.D. Vermulen (1984a). "Continuous Flow Gas Lift: Heading Action Analyzed for Stabilization". *Oil Gas Journal* 82.31.

Grupping, A.W., C.W.F. Luca, and F.D. Vermulen (1984b). "Continuous Flow Gas Lift: These Methods Can Eliminate or Control Annulus Heading". *Oil Gas Journal* 47.51.

Hu, B. and M. Golan (2003). "Gas-Lift Instability Resulted Production Loss and Its Remedy by Feedback Control: Dynamical Simulation Results". *SPE International Improved Oil Recovery Conference in Asia Pacific, 20-21 October, Kuala Lumpur, Malaysia. SPE 84917*.

Kreyszig, E. (2011). *Advanced Engineering Mathematics*. 10th. John Wiley & sons, inc., pp. 474–532.

Larsen, C. A. and H. A. Asheim (2014). "Experimental Investigation of Gas Lift Instability and Dynamic Regulation to Control It". *SPE Annual Caspian Technical Conference and Exhibition, 12-14 November, Astana, Kazakhstan. SPE 172271*.

"Norskehavskonferansen" (08.03.2017). H. Skofteland, R. Tittel, and E. Meyer.

NorskPetroleum (2017). *Heidrun*. URL: http://www.norskpetroleum.no/en/facts/field/heidrun/.

NPD (2016). *NPD Factpages, Heidrun*. URL: http://factpages.npd.no/FactPages/default.aspx?nav1=field&nav2=PageView%7CAll&nav3=43771&culture=en.

Poblano, E., R. Camacho, and Y. V. Fairuzov (2002). "Stability Analysis of Continuous-Flow Gas Lift Wells". *SPE Annual Technical Conference and Exhibition, 29 September-2 October, San Antonio, Texas. SPE 77732*.

Schlumberger (2016). *Oilfield Glossary, water formation volume factor*. URL: http://www.glossary.oilfield.slb.com/Terms/w/water_formation_volume_factor.aspx.

Al-Shemmeri, T. (2012). *Engineering Fluid Mechanics*. Bookboon, pp. 17–18.

Smith, C. A. and A. B. Corripio (1997). *Principles and Practice of Automatic Process Control*. 2nd. John Wiley & sons, inc., pp. 6, 287.

Standing, M.B. (1947). "A Pressure-Volume-Temperature Correlation for Mixtures of California Oils and Gases". *Drilling and Production Practice*. American Petroleum Institute.

Statoil (2015). *Statoil Operated Fields in Norway, Heidrun*. URL: http://www.statoil.com/en/OurOperations/ExplorationProd/ncs/heidrun/Pages/default.aspx.

Sutton, R. P. (1985). "Compressibility Factors for High-Molecular-Weight Reservoir Gases". *SPE Annual Technical Conference and Exhibition, 22-26 September, Las Vegas, Nevada. SPE 14265*.

Tokar, T., Z. Schmidt, and C. Tuckness (1996). "New Gas Lift Valve Design Stabilizes Injection Rates: Case Studies". *SPE Annual Technical Conference and Exhibition, 6-9 October, Denver, Colorado. SPE 36587*.

Walsh, M. P. (2007). *Petroleum Engineering Handbook*. Ed. by L. W. Lake and E. D. Holstein. Society of Petroleum Engineers. Chap. Volume V, Reservoir Engineering and Petrophysics, p. 700.

Whitson, C. H. and M. R. Brulé (2000). *Phase Behaviour*. Society of Petrolum Engineers, Henry L. Doherty series, pp. 22–35.

Wiggins, M. L. (1993). "Generalized Inflow Performance Relationships for Three-Phase Flow". *SPE 25458*.

Wikipedia, the free encyclopedia (2016). *Nyquist Frequency*. URL: https://en.wikipedia.org/wiki/Nyquist_frequency.

Winkler, H. W. and J. R. Blann (2007). *Petroleum Engineering Handbook*. Ed. by L. W. Lake and J. D. Clegg. Society of Petroleum Engineers. Chap. Volume IV, Production Operations Engineering, p. 538.

Xu, Z. G. and M. Golan (1989). "Criteria for Operation Stability and Gas-Lift Wells". *SPE 19362*.

Yarborough, L. and K.R. Hall (1974). "How to Solve Equation of State for Z-Factors?" *Oil & Gas Journal* 72, pp. 86–88.

Zuber, A. and B. Finlay (1965). "Average Volumetric Concentration in Two-Phase Flow Systems". *Journal of Heat Transfer Ser. C. 87, 453*.

Appendix A

Figures

The data of the liquid flow rate are illustrated in the figures in this appendix. The flow rate is plotted in black and the exponential weighted moving average is found in red in all of the figures presented.

Figure A.1 shows the production in January and February 2016. The highly oscillating period in February 2016, which was used to evaluate the stationary model in Chapter 8.1.1, is found at $t = 1002 - 1153$ hrs in Figure A.1.

Figure A.2 shows the production in March and April 2016. The period in $t = 48 - 413$ hrs, which is affected by noise, and the highly oscillating period in $t = 562 - 1153$ hrs were used in the analysis in Chapter 8.1.1.

Figure A.3 illustrates the production in May and June 2016. In Chapter 8.1.1 were the highly oscillating period in $t = 220 - 430$ hrs in May used to compare the model to real data.

Figure A.4 shows the production in July and August 2016.

Figure A.5 shows the production in September and October 2016. The low amplitude period in $t = 758 - 1100$ hrs were used in Chapter 8.1.1.

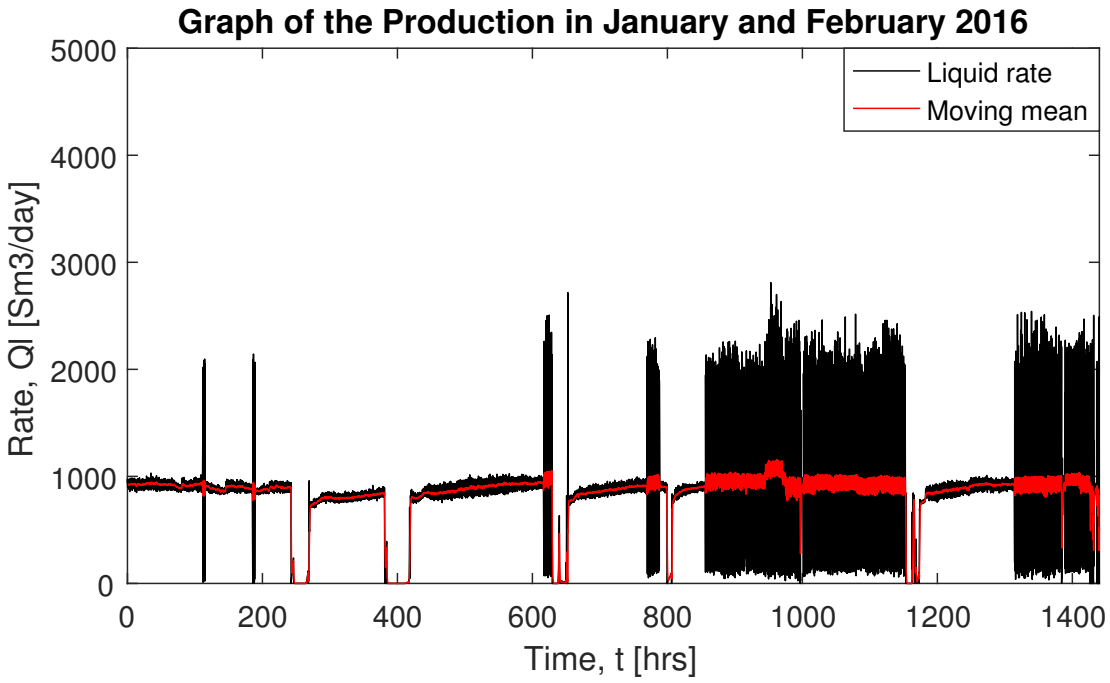

Figure A.1: Liquid production in January and February 2016.
$t = 1002 - 1153$ hrs is used in the comparison in Chapter 8.1.1.

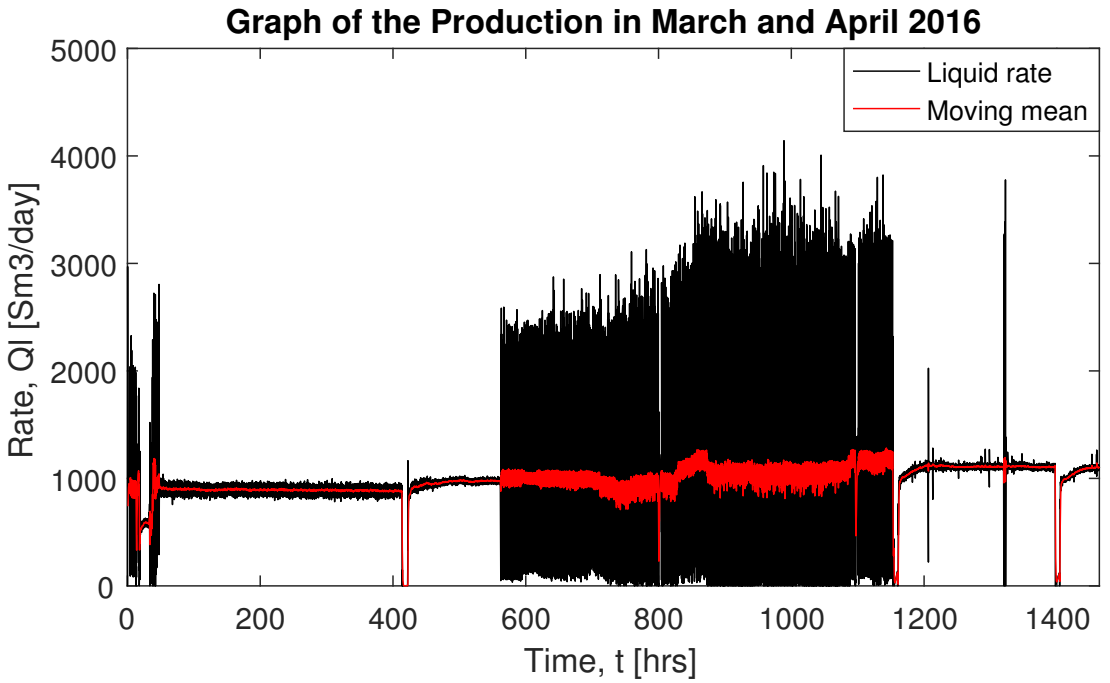

Figure A.2: Liquid production in March and April 2016.
$t = 48 - 413$ hrs and $t = 562 - 1153$ hrs are used in the comparison in Chapter 8.1.1.

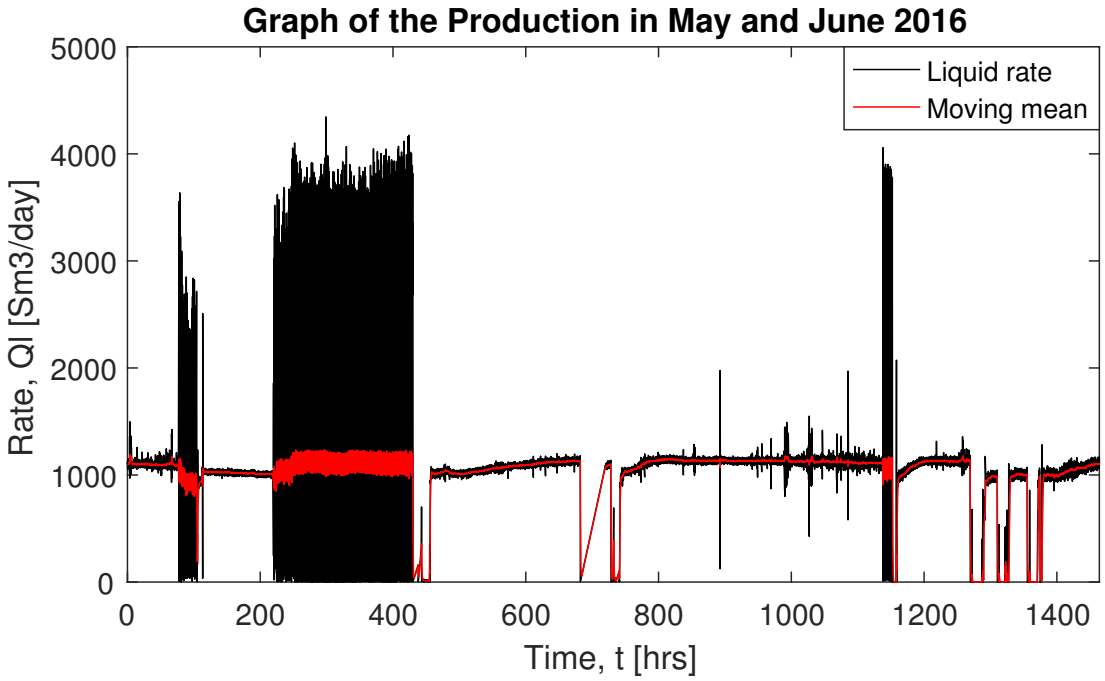

Figure A.3: Liquid production in May and June 2016.
$t = 220 - 430$ hrs is used in the comparison in Chapter 8.1.1.

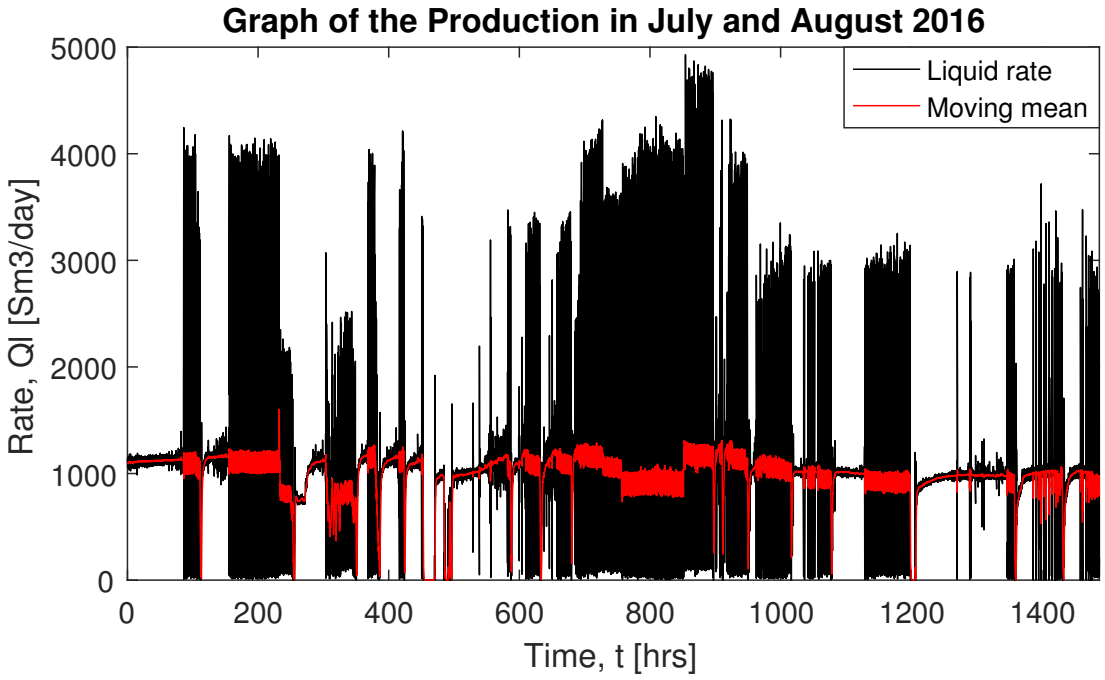

Figure A.4: Liquid production in July and August 2016.

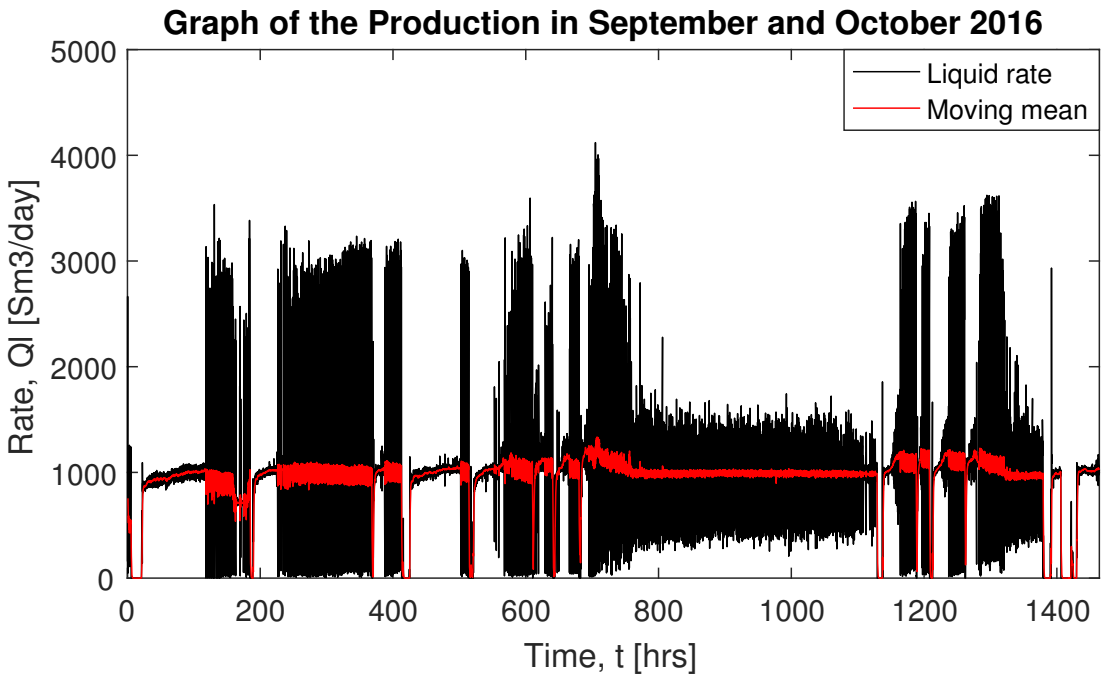

Figure A.5: Liquid production in September and October 2016.
$t = 758 - 1100$ hrs is used in the comparison in Chapter 8.1.1.

Appendix B

Derivations

More details on the mathematical derivations done in the thesis.

Choke Flow Relationship

The flow equation becomes $dp + \rho v dv = 0$ when the acceleration forces dominates. Integrating this equation over the orifice results in

$$p_i = p_a - \frac{1}{2}\rho_g \left(v_i^2 - v_a^2\right), \tag{B.1}$$

where the subscript a indicates the inlet of the orifice, which is in the annular space between casing and tubing. The subscript i denotes the pressure and velocity right after the outlet of the nozzle.

To obtain a relationship between the orifice and the tubing, a Borda-Carnot based pressure recovery balance is used:

$$Ap_t + \dot{m}v_t = Ap_i + \dot{m}v_i, \tag{B.2}$$

where $\dot{m} = \rho_g v_i A$. Rearranging Equation B.2, the tubing pressure is expressed as

$$p_t = p_i + \rho_g \left(v_i^2 - v_t v_i\right). \tag{B.3}$$

Inserting Equation B.1 in Equation B.3, the pressure reduction across the choke is

$$p_a - p_t = \frac{1}{2}\rho_g \left(v_i^2 - v_a^2\right) - \rho_g \left(v_i^2 - v_t v_i\right).$$

With $v = Q/A$ and assuming a slightly compressible fluid and an equal cross-sectional area of the tubing and the annulus, it follows that $v_a = v_t$. The pressure reduction can then be expressed as

$$\begin{aligned} p_a - p_t &= \frac{1}{2}\rho_g \left(2v_i v_t - v_i^2 - v_t^2\right) \\ &= \frac{1}{2}\rho_g \left(2\frac{Q^2}{A_t A_i} - \frac{Q^2}{A_i^2} - \frac{Q^2}{A_t^2}\right) \\ &= \frac{1}{2}\rho_g \left(\frac{Q}{A_i}\right)^2 \left(1 - \frac{A_i}{A_t}\right)^2. \end{aligned}$$

For a port size that is much smaller than the cross-sectional area of the pipe ($A_i \ll A_t$), the final expression for the choke flow relationship is seen in Equation B.4.

$$p_a - p_t = \frac{1}{2}\rho_g \frac{Q_g^2}{A_i^2}. \tag{B.4}$$

Dynamical Response

Coefficients

Tubing Response

The tubing pressure response to any disturbance is given by the steady state pressure drop along the tubing:

$$\frac{\partial}{\partial t}\delta p_w f = gL\frac{\partial}{\partial t}\overline{\rho}_{tp} + \frac{f\overline{\rho}_m \overline{v}_m L}{d}\frac{\partial}{\partial t}\delta\overline{v}_m. \tag{B.5}$$

Thus, the tubing response is dependent on the density and velocity changes.

The equation for the two-phased mixture density is $\rho_{tp} = \rho_g y_g + \rho_l y_l$, where $y_g = 1 - y_l$.

The liquid holdup, y_l, is a function of the superficial velocities, v_{sl}, v_{sg},

$$\delta y_l = \frac{y_l}{v_m}\delta v_{sl} - \frac{y_g}{v_m}\delta v_{sg}. \tag{B.6}$$

The change in two-phased density from inlet to outlet can be written in terms of liquid holdup and time delay, seen in Equation B.7

$$\frac{\partial}{\partial t}\delta\overline{\rho}_{tp} = \frac{\Delta\rho v_c}{L}\left(\delta y_l\right)_t^{t+\Delta t}. \tag{B.7}$$

By inserting Equation B.6 in B.7, the density change is related to change in the superficial velocities:

$$\frac{\partial}{\partial t}\delta\overline{\rho}_{tp} = \frac{\Delta\rho v_c}{L v_m}\left(y_l\delta v_{sl} - y_g\delta v_{sg}\right)_t^{t+\Delta t}. \tag{B.8}$$

A change in the inflow mixture velocity will immediately affect the whole tubing, and Equation B.9 is a relation between the change in mixture velocity and inflow rates.

$$\delta\overline{v}_m = \frac{1}{A_t}\left(\beta_g\delta Q_g + \beta_o\delta Q_o\right). \tag{B.9}$$

Inserting Equation B.8 and B.9 in B.5, the tubing response will be related to liquid holdup and changes in the inflow rate.

$$\frac{\partial}{\partial t}\delta p_w f = \frac{\Delta\rho g L v_c}{V_t v_m}\left(y_l\delta Q_l - y_g\delta Q_g\right)_t^{t+\Delta t} + \frac{f\overline{\rho}_m v_m L}{\pi d^3}\left(\frac{\partial}{\partial t}\beta_o\delta Q_o + \frac{\partial}{\partial t}\beta_g\delta Q_g\right). \tag{B.10}$$

Annular Response

The annulus is considered as a compressible gas volume, thus, the pressure response can be described by the equation $\frac{\partial}{\partial t}\delta p_g = -\beta_a\frac{p_g}{V_r}\delta Q_g$. The inflow of lift-gas is affected by the pressure drop across the downhole orifice, that is: $\delta Q_g = \frac{A_i^2}{\rho_g Q_g}\left(\delta p_g - \delta p_w f\right)$. Combined, the annulus response is described as

$$\frac{\partial}{\partial t}\delta p_g = \frac{\beta_a p_g A_c^2}{V_t\rho_g Q_g}\left(\delta p_w - \delta p_g\right). \tag{B.11}$$

System Response

By combining Equation B.10 and B.11 the system response matrix can be written as

$$\frac{\partial}{\partial t}\begin{bmatrix}\delta p_w f\\ \delta p_g\end{bmatrix} = \begin{bmatrix}a_w & -a_g\\ c & -c\end{bmatrix}\begin{bmatrix}\delta p_w f\\ \delta p_g\end{bmatrix}_t + \begin{bmatrix}d_w & -d_g\\ 0 & 0\end{bmatrix}\begin{bmatrix}\delta p_w f\\ \delta p_g\end{bmatrix}_{t+\Delta t} \tag{B.12}$$

where the coefficients $a_w,\ a_g,\ c,\ d_w,\ d_g$ can be determined by the well parameters.

$$\begin{aligned}
a_w &= \alpha\left(J_g K_g - J K_l + F_g J_g^2 K_a\right)\\
a_g &= \alpha\left(J_g K_g + F_g J_g^2 K_a\right)\\
c &= J_g K_a\\
d_w &= \alpha\left(J_g K_g - J K_l\right)\\
d_g &= \alpha J_g K_g\\
\alpha &= \left(1 + F_g J_g + F_l J\right)^{-1},
\end{aligned}$$

where K_g and K_l means density response to gas and liquid flow, F_g and F_l means friction response along tubing to gas and liquid flow and the K_a is a annular pressure response relation. J is the usual productivity index and J_g is the gas injection index.

The response parameters above have the following relationship to the well parameters:

$$\begin{aligned}
K_g &= \frac{\Delta\rho g L}{V_t}\frac{v_c}{v_m}y_g, & K_l &= \frac{\Delta\rho g L}{V_t}\frac{v_c}{v_m}y_l,\\
F_g &= \frac{4f\overline{\rho}_m\overline{v}_m L}{\pi d^3}\beta_g, & F_l &= \frac{4f\overline{\rho}_m\overline{v}_m L}{\pi d^3}\beta_o,\\
J &= \frac{Q_l}{p_r - p_{wf}}, & J_g &= \frac{A_i^2}{\rho_g Q_g},\\
K_a &= \beta_a\frac{p_g}{V_r},
\end{aligned}$$

where β_g and β_o denotes the expansion between tubing average and downhole conditions: $\beta_g = \overline{B}_g/B_g$ and $\beta_o = \overline{B}_o/B_o$. β_a, on the other hand, accounts for the gas formation volume factor between annular average and downhole conditions, $\beta_a = \overline{B}_{ga}/B_{ga}$.

Relation to Stability Criterion

The dynamical response model in Chapter 6 relates to Asheim (1988) criteria in Chapter 2.2.2.

The dynamical response model consider both inflow and outflow. Neglecting the delayed outflow response $t + \Delta t$, the matrix simplifies to

$$\frac{\partial}{\partial t}\begin{bmatrix}\delta p_w f \\ \delta p_g\end{bmatrix} = \begin{bmatrix}a_w & -a_g \\ c & -c\end{bmatrix}\begin{bmatrix}\delta p_w f \\ \delta p_g\end{bmatrix}_t \tag{B.13}$$

which has the eigenvalues

$$\lambda = 0.5(a_w - c) \pm 0.5\sqrt{(a_w - c)^2 - 4(a_g - a_w)c}. \tag{B.14}$$

Since $a_g > a_w$ the expression under the square-root will usually be negative, hence, the eigenvalues will have the form

$$\lambda = \alpha \pm i\omega = 0.5(a_w - c) \pm i0.5\sqrt{(a_w - c)^2 - 4(a_g - a_w)c} \tag{B.15}$$

and the matrix B.13 will have decoupled solutions on the form $\delta p_{w,g}(t) = \delta p^0_{w,g}(e^{(\alpha+i\omega)t}$ (Asheim, 2016). For the system to be dynamical stable the real part of the eigenvalues, α, must be negative. Accordingly, $\alpha = a_w - c < 0$, which corresponds to Asheim (1988) F_2 criterion (Chapter 2.2.2)

$$c/a_w = \frac{V_t}{V_a}\frac{p_g}{\Delta\rho g L}\frac{Q_g + Q_o}{Q_o}\frac{1}{1 - F_1} > 1, \quad \text{where} \quad F_1 = \frac{B_o J}{Q_o}\frac{\rho_g Q_g^2}{A_i^2} > 1. \tag{B.16}$$

Appendix C

Matlab

The code used to compute the stationary model and the pressure response in chapter 4 and 6 are presented in this appendix. The other functions and script are submitted in a zip-file along with the thesis.

Stationary Model

Numerical integration of the tubing pressure and the annular pressure from the wellhead down to the reservoir.

```
clear
PeriodStableJan;          % Considered period
WellSpecifications        % From given well specifications

%Gas distribution factor depends on the deviation in the rate
if sigma < 600
    Co=1.30;
elseif sigma > 600 && sigma < 850
    Co=1.36;
elseif sigma > 850 && sigma < 1000
```

```
11      Co=1.43;
12  elseif sigma > 1000 && sigma < 1300
13      Co=1.55;
14  else
15      Co=1.60;
16  end
17
18  myg= 1e-5;                  % Pa*s   Viscosity of gas guess
19  Twh= mean(twh);             % C      Wellhead temperature
20  Tgrad=(Tres-Twh)/Lres;      % C      Geothermal gradient
21
22  %--------------Preallocating--------------------
23  k= 1;                       %        k=i-1, the previous value
24  Preallocating
25  wor=mean(qw)/(mean(qw+qo));
26  %---Numerical Integration of the pressure along annulus---
27  % At the wellhead:
28  Pg(1)=mean(pgi)*10^5;
29  T=Twh+Tgrad*1+274.15;
30  [Bga(1),rhoga(1)]=FVFannulus(gg,T,Pg(1));
31  Qga(1)=Qg_i*Bga(1);
32  % Along the rest of the annulus:
33  for i=2:Lres    % annulus
34      T=Twh+Tgrad*i+274.15;              % K      Temperature at i
35      [Bga(i),rhoga(i), z]=FVFannulus(gg,T,Pg(k));%Annular gas FVF
36      Qga(i)=Qg_i*Bga(i);                % m3/s   Gas rate in annulus
37      if i<=Linj                         %        Above the gas valve
38          Pg(i)=Pg(k)+g*rhoga(i);        % Pa     Gas pressure in
                annulus
39      else                               %        Below the gas valve
```

```
40          Pg(i)=Pg(k)+g*rhow;          % Pa     Pressure in annulus
41      end
42       Qg_inj=Qga(Linj);               %       Lift gas rate at Linj
43       k=k+1;                          %       Counter
44  end
45  k=1;                                 %       Reset counter
46
47  %-----Numerical Integration of the pressure along tubing-------
48  % At the tubing head:
49  p(1)=pth;
50  T=Twh+Tgrad*1+274.15;
51  [Bg(1), Bo(1), rhoo, rhog, Rs(1)] = FVF (go, gg, T, p(1));
52  Qg_tbg(1)=Qg_r*Bg(1);
53  yl(1)= 0.145;
54  yg(1)=1-yl(1);
55  vsg(1)=Qg_tbg(1)/At;
56  vsl(1)=mean(qw+qo*Bo(1))/(24*60*60)/At;
57  % In the rest of the tubing:
58  for i=2:Lres     % tubing
59      T=Twh+Tgrad*i+274.15;            % K      Temperature at i
60      myo=6e-8*(p(k)/10^5)^2-3.01e-5*p(k)/10^5+6.3348e-3;% Pa*s
            Oil viscosity
61      [Bg(i),Bo(i),rhoo,rhog,Rs(i)]=FVF(go,gg,T,p(k));% FVF
62      Qo(i)=mean(qo)/(24*60*60)*Bo(i);% m3/s  Oil rate
63      Ql(i)=mean(qw)/(24*60*60)+Qo(i);% m3/s  Liquid rate
64      if i<=Linj                       %       Above gas valve
65          Qg_tbg(i)=Qg_r*Bg(i);        % m3/s  Gas rate in tubing
66      else                             %       Below gas valve
67          Qg_tbg(i)=Qg_r*Bg(i)-Qg_inj;% m3/s  Gas rate in tubing
68      end
```

```
69        rhol=rhoo*(1-wor)+rhow*wor;          % kg/m3 Density of oil+water
70        vsg(i)=Qg_tbg(i)/At;                 % m/s    Gas superficial v.
71        vsl(i)=Ql(i)/At;                     % m/s    Liquid superficial v.
72        vm(i)=vsl(i)+vsg(i);                 % m/s    Mixture velocity
73        vc(i)=Co*vm(i);                      % m/s    Kinematic velocity
74        yl(i)=0.5*sqrt((vsg(i)/vo+Co*vsl(i)/vo-1)^2+4*Co*vsl(i)/vo)
              -0.5*(vsg(i)/vo+Co*vsl(i)/vo-1);%    Liquid fraction
75        yg(i)=1-yl(i);                       %       Gas fraction
76        rhotp(i)=rhol*yl(i)+rhog*yg(i);      % kg/m3 Density of two-phase
77        myw=2.414e-5*10^(247.8/(T-140));     % Pa*s   Water viscosity
78        myl=myo*(1-wor)+myw*wor;             % Pa*s   Liquid viscosity
79        my=myl*yl(i)+myg*yg(i);              % Pa*s   Mixture viscosity
80        Re=rhotp(i)*vm(i)*d/my;              %       Reynolds number
81        f(i)= Af*Re^(-Bf);                   %       Friction factor
82        p(i)=p(k)+g*rhotp(i)+0.5*f(i)*rhotp(i)/d*vm(i)^2;%Pa Pressure
83        k=k+1;                               %       Counter
84    end
85    k=1;                                     %       Reset counter
86
87    %---Compare Measured Pw (MFM) and the calculated p(Lmfm)----
88    pw=mean(pwf);                            % Pa     Wellbore pressure
89    err=(pw-p(Lmfm)./10^5);                  % Bar    Diff pressure
90
91    Vtry=[Co, Af, Bf, err, p(Lmfm)./10^5, Ql(Lmfm)*24*60*60, (err/pw)
          *100]
92    %---Plot of the well pressure and annulus pressure vs depth-----
93    maxP=200;
94    InjDepth=-Linj*ones(1,maxP);             % L       Gas valve depth
95    MFMDepth=-Lmfm*ones(1,maxP);             % L       Gauge carrier depth
96    ResDepth=-Lres*ones(1,maxP);             % L       Casing depth
```

```
97  xp=[1:maxP]-1;
98  figure(1)
99  plot(xp,InjDepth,'--r',xp,MFMDepth,'--g',xp,ResDepth,'--m',p(1:
        Lres)./10^5,-(1:Lres),'b',Pg(1:Lres)./10^5,-(1:Lres),'r')
100 axis([0 200 -3000 0])
101 legend('Injection Depth','Measurement Depth', 'Reservoir Depth');
102 title('Pressure Profile');
103 xlabel('\bf Pressure [bar]');
104 ylabel('\bf Depth [m]');
105 grid
106 %-------Plot of the superficial velocities vs depth---------
107 maxV=10;
108 InjDepth=-Linj*ones(1,maxV);          % L      Gas valve depth
109 MFMDepth=-Lmfm*ones(1,maxV);          % L      Gauge carrier depth
110 ResDepth=-Lres*ones(1,maxV);          % L      Casing depth
111 xv=[1:maxV]-1;
112 figure(2)
113 plot(-(1:Lres),vsg,-(1:Lres),vsl,InjDepth,xv,'--r',MFMDepth,xv,'
        --g',ResDepth,xv,'--m')
114 legend('Gas','Liquid');
115 title('Velocity Profile');
116 xlabel('\bf Depth [m]');
117 ylabel('\bf Velocity [m/s]');
118 grid
119 %----------Plot of the liquid fraction vs depth--------
120 maxV=2;
121 InjDepth=-Linj*ones(1,maxV);          % L      Gas valve depth
122 MFMDepth=-Lmfm*ones(1,maxV);          % L      Gauge carrier depth
123 ResDepth=-Lres*ones(1,maxV);          % L      Casing depth
124 xv=[1:maxV]-1;
```

```
125 figure(3)
126 plot(xv,InjDepth,'--r',xv,MFMDepth,'--g',xv,ResDepth,'--m',yg
      ,-(1:Lres),'b')
127 legend('Injection Depth','Measurement Depth', 'Reservoir Depth');
128 title('Liquid Fraction vs Depth');
129 xlabel('\bf Liquid fraction');
130 ylabel('\bf Depth [m]');
131 grid
```

Response Model

```
%————————Dynamical response system————————————————
%StasjModellTrykk          % Calculate the variables along tbg

%————————Calculating the coefficients————————————————
betaa=mean(Bga)/Bga(Linj);      % Ratio of average and downhole Bg
    in annulus
Ka= mean(Pg)/Va*betaa;          % Annular pressure response
% Density Response:
Ko=(rhoo-rhog)*g*Lres/Vt*vc(Lres)/vm(Lres)*yl(Lres);
Kg=(rhoo-rhog)*g*Lres/Vt*vc(Lres)/vm(Lres)*yg(Lres);
% Friction Response:
Fo=4*mean(f)*mean(rhotp)*mean(vm)*Lres/pi/d^3*mean(Bo)/Bo(Lres);
Fg=4*mean(f)*mean(rhotp)*mean(vm)*Lres/pi/d^3*mean(Bg)/Bg(Lres);
Jg=Ac^2/rhog/Qg_tbg(Lres);  % Gas injection index
delta_t=Lres/mean(vc);          % s Time delay

% Matrix Coefficients:
a1=(Jg*Kg-J*Ko+Fg*Jg^2*Ka)/(1+ Fg*Jg +Fo*J);
b1=(Fg*Jg^2*Ka+Jg*Kg)/(1+ Fg*Jg +Fo*J);
c= Jg*Ka;
a2=(Jg*Kg-J*Ko)/(1+ Fg*Jg +Fo*J);
b2=(Jg*Kg)/(1+ Fg*Jg +Fo*J);

%————————Plot of dynamical response system————————————
delT=delta_t; % s tidsforsinkelse
disp('——— Response coefficients ————————')
fprintf(' a1= %12.4e b1= %12.4e c= %12.4e a2= %12.4e b2= %12.4e\n
    ',a1,b1,c,a2,b2)
```

```
27 disp([' delT =',num2str(delT/60),' (minute)'])
28 tmax=60*60*3;
29 t=linspace(0,tmax);
30 %------------------------ diff ------------------
31 A=[a1, -b1; c, -c] ;
32 ddefun  = @(t,x) A*x;
33 [tv,pdyn]=ode45(ddefun,[0,tmax],[1;-1]);
34 subplot(2,1,1)
35 plot(tv/60,pdyn(:,1),tv/60,pdyn(:,2))
36 title('Pressure response 01.01-18.01.2017')
37 legend('Well bottom','Annulus')
38 xlabel('\bf Time [min]')
39 ylabel('\bfPressure [Pa]')
40 axis([0 tmax/60 -5 5])
41 grid
42 %------------------------ del-diff-------------------------
43 D=[-a2, b2; 0,0];
44 ddedel  = @(t,x,xdelay) A*x-D*xdelay;
45
46 sol=dde23(ddedel,delT,[1;-1],[0,tmax]);
47 yint = deval(sol,t);
48 qoplot=yint(2,:);
49 qgplot=yint(1,:);
50 subplot (2,1,2)
51 plot(t/60,qoplot,t/60,qgplot);
52 legend('Well bottom','Annulus')
53 xlabel('\bf Time [min]')
54 ylabel('\bfPressure [Pa]')
55 axis([0 tmax/60 -5 5])
56 grid
```